

AD-A124 879

PASSIVE FILMS SURFACE STRUCTURE AND STRESS CORROSION  
AND CREVICE CORROSION. (U) NATIONAL BUREAU OF STANDARDS  
WASHINGTON DC J KRUGER ET AL. FEB 83 NBSIR-83-2551  
NAONR-18-69

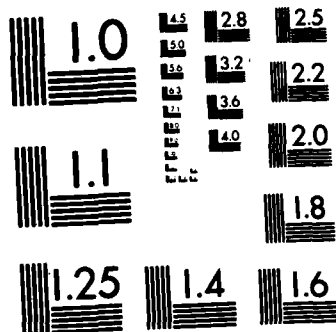
1/1

UNCLASSIFIED

F/G 11/6

NL


END  
FILMED  
F  
DTIC



MICROCOPY RESOLUTION TEST CHART  
NATIONAL BUREAU OF STANDARDS-1963-A

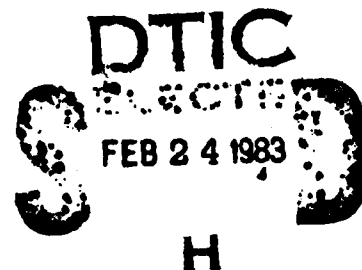
(12)

NBSIR 83-2551

# **Passive Films, Surface Structure and Stress Corrosion and Crevice Corrosion Susceptibility**

---

U.S. DEPARTMENT OF COMMERCE  
National Bureau of Standards  
Inorganic Materials Division  
and  
Metallurgy Division  
Washington, DC 20234



November 1982

DISTRIBUTION OF THIS DOCUMENT IS UNLIMITED

Issued February 1983

DTIC FILE COPY

Prepared for  
Office of Naval Research  
Department of the Navy  
Arlington, VA 22217

83 02 024 008

NBSIR 83-2551

**PASSIVE FILMS, SURFACE STRUCTURE  
AND STRESS CORROSION AND CREVICE  
CORROSION SUSCEPTIBILITY**

---

J. Kruger, J.J. Ritter, and G.G. Long

U.S. DEPARTMENT OF COMMERCE  
National Bureau of Standards  
Inorganic Materials Division  
and  
Metallurgy Division  
Washington, DC 20234

November 1982

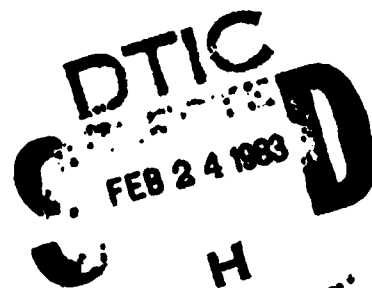
DISTRIBUTION OF THIS DOCUMENT IS UNLIMITED  
Issued February 1983

Prepared for  
Office of Naval Research  
Department of the Navy  
Arlington, VA 22217



---

**U.S. DEPARTMENT OF COMMERCE, Malcolm Baldrige, *Secretary***  
**NATIONAL BUREAU OF STANDARDS, Ernest Ambler, *Director***



ELLIPSOMETRIC STUDIES ON THE CATHODIC DELAMINATION OF  
ORGANIC COATINGS ON IRON AND STEEL

Joseph J. Ritter  
Materials Chemistry Division  
National Bureau of Standards  
Washington, D.C. 20234

Abstract

A number of mechanisms have been proposed to explain the cathodic delamination of organic coatings from iron or steel undergoing corrosion. Ellipsometric studies carried out on these substrates protected by either collodion, acrylic lacquers, or polybutadiene indicate that dissolution of the interfacial oxide in the highly alkaline cathodic environment constitutes the predominant mode of delamination. Moreover, the spatial development of cathodic areas has been probed both ellipsometrically and through subcoating electrochemical pH measurements.

The oxide dissolution proposition is supported by independent experiments with uncoated iron in a highly alkaline medium.

Key words: Air-formed oxide films; cathodic delamination; ellipsometry;  
organic coatings; pH measurements



Accession For	
DTIC	ORNL
DTIC	TR
Unannounced	
Justification	
By	
Distribution/	
Availability Codes	
Dist	Material and/or
	Contract
A	

# ELLIPSOMETRIC STUDIES ON THE CATHODIC DELAMINATION OF ORGANIC COATINGS ON IRON AND STEEL

Joseph J. Ritter  
Materials Chemistry Division  
National Bureau of Standards  
Washington, D.C. 20234

## Introduction

The corrosion related failure of organic coatings on iron or steel is brought about through two destructive processes, the anodic dissolution of metal and the cathodic delamination of the coating. The development and effects of these phenomena have been treated in detail by a number of workers [1-4]. While in a practical sense, the anodic dissolution of metal is relatively well understood, the mechanisms for coating delamination are still not resolved. For example, previous authors have proposed various delamination mechanisms ranging from an active role by water molecules in displacing substrate-polymer bonds to cohesive failure of the polymer [5-7]. Each of these ideas can be supported by experimental evidence from specific coating-substrate systems. Thus, perhaps it is most reasonable to consider a predominant mode of delamination in connection with a given coating-substrate system. The purpose of the study described here is to present evidence for yet another mechanism of delamination, the dissolution or alteration of the interfacial air-formed oxide films\*.

In an earlier publication from our laboratory we suggested this possibility based on ellipsometric observations of the iron/collodion system [3]. Workers at Lehigh University have arrived at a similar conclusion for other systems through independent means [9]. We have shown in previous work

---

\*For the purpose of this publication, the term "air-formed oxide film" refers to the oxide present on the metal surface at the end of the surface preparation regimen.

how qualitative ellipsometry combined with electrochemical pH measurements and microanalyses can provide valuable information about subcoating phenomena and chemistry [4,8,10]. While this early work focused on the iron/collodion system, the results presented in this report are derived from both iron and steel substrates protected by either collodion, polystyrene, acrylic lacquers, or polybutadiene. In addition, the use of our newly automated ellipsometer system [11] has provided detailed insights into the real time evolution of the phenomena surrounding cathodic delamination. The interpretations are supported by independent experiments, described here, with uncoated iron in simulated subcoating environments.

### Experimental

All iron specimens were mounted in epoxy and finished on a series of SiC papers of 320, 400, and 600 grit. Final polishing was done with 6, 1, and 0.05  $\mu\text{m}$  abrasives.

Low carbon stamping quality steel kindly supplied by Dr. Henry Leidheiser, Jr., Lehigh University, as 0.71 mm sheet, was used with the as-received 600 grit finish. The sheets were sectioned into 2 cm squares, coated, and cast in epoxy in a recessed manner, so that only one face of the material was exposed. Dr. Leidheiser also supplied specimens of this same steel with 20  $\mu\text{m}$  of heat-cured polybutadiene applied. The coated specimens were mounted in epoxy in a similar recessed fashion.

With respect to other coating materials, collodion was diluted 1:1 with methanol, while the polystyrene, and two proprietary acrylics, designated A and B were dissolved and/or thinned with toluene. These materials were applied by dipping, usually resulting in a 25 to 100  $\mu\text{m}$  cured coating after 18 h at room temperature (22 to 25  $^{\circ}\text{C}$ ). Heat-cured acrylic coatings were prepared in the same manner but subjected to 200  $^{\circ}\text{C}$  for 40 min after the 18 h room temperature cure.

The details of specimen arrangement and the ellipsometric technique have been described previously [8,10]. In brief, the technique involves the passage of elliptically polarized light through the transparent coating and reflection from the substrate surface. In some experiments a miniature pH probe is used to simultaneously monitor the environment at the coating-substrate interface. Changes in the phase ( $\delta\Delta$ ) and amplitude ( $\delta\Psi$ ) of the reflected light have been shown to be indicative both of alterations in surface texture (roughness) and changes in the thickness of the surface oxide film. Thus, the technique is of value in studying the behavior of the substrate under the coating as the corrosion process proceeds.

All coated specimens were studied immersed in 0.05 M NaCl at 25 °C. Uncoated iron specimens were examined in aerated, saturated NaOH at 25 °C. The corrosion process was initiated by damaging the coating in a single area with either a 0.07 cm drill point or incising a 1 mm slit with a scalpel.

Preparation of segmented specimens. Segmented specimens were devised as one means to examine the spatial development of subcoating-cathodes. This technique permits the initial isolation of remote and proximate (relative to an anode) cathodes for independent study. A 1 cm diameter x 1 cm long iron cylinder was divided into two parts, each part fitted with a copper conductor and cast into a single epoxy slug as shown in figure 1. An opening was drilled through one of the segments (c), to accommodate a miniature (1.5 mm dia.) pH probe. The drilled hole was temporarily closed with a polytetrafluoroethylene plug and the entire slug face coated with acrylic lacquer "A" which was air-cured at 25 °C for 18 h. The specimen was mounted horizontally in an ellipsometer cell immersed in 0.05 M NaCl. The cell mount permitted horizontal translation of the specimen so that either segment a or c could be examined ellipsometrically.



## Results and Discussion

### General Effects of Coating Cure Procedure

Figures 2 and 3 schematically show the responses of the ellipsometric phase retardation ( $\Delta$ ) parameter with time for coated iron and steel specimens. For the room temperature cured coatings, the curve shapes are similar but the heat-cured coatings show a very different ellipsometric response. The interpretation of these responses with respect to subcoating phenomena are given below.

### Ellipsometric Responses for Room Temperature Cured Coatings

Figures 4, 5, and 6 show the detailed real time behavior of the ellipsometric parameters  $\Delta$  and  $\Psi$  for room temperature cured collodion and the two types of proprietary acrylic coatings. Overall, the curves show similar behavior on different time scales. Since the coated metal systems are optically quite complex, the ellipsometric results are examined in a qualitative sense [10].

Within Region I each of the three systems show a rise in  $\Delta$  and a concomitant decline in  $\Psi$  as corrosion sets in. We interpret this type of behavior as a change in oxide film thickness and the direction of change is indicative of a film thinning process. The interpretation of the  $\Delta$  and  $\Psi$  changes is derived from the behavior of these parameters for uncoated iron in saturated NaOH (cf. fig. 10). Saturated NaOH represents a reasonable subcoating environment based on in situ pH measurements [8]. We relate these changes to the dissolution of the oxide film in the highly alkaline cathodic environment. Since the coating is bonded to this oxide layer, delamination has occurred.

Within Region II,  $\Delta$  and  $\Psi$  decline sharply in concert. This concerted response is typical of a change in surface texture (roughening). The interpretation of the behavior of  $\Delta$  and  $\Psi$  is based on our observations of

uncoated iron in borate buffer solution after potential cycling [8], which, in effect, gives a smoother surface. In the potential cycling experiments  $\Delta$  and  $\Psi$  rise in concert, the opposite effect from that observed for coated metals. Since phenomenon described in Region I was a thinning of the oxide layer, it is reasonable to postulate the presence of patches of film-free metal. The high pH environment promotes direct metal dissolution from these patches and the surface becomes roughened.

Within Region III,  $\Delta$  and  $\Psi$  are again in opposition. The overall result is indicative of an increase in film thickness. Since the phenomena in Regions I and II resulted in the dissolution of iron either from the oxide or from the metal itself, we postulate that soluble iron species\*, like the  $\text{OH}^-$  ions, accumulate under the coating. Ultimately, solubility product constants are exceeded and precipitation occurs. The complexity of the ellipsometric response in Region III for figures 4 and 5 may arise from one or both of the following factors: the deposition of metastable films which partially redissolve and reprecipitate until a stable format is achieved; or the precipitation of a film which undergoes massive changes in its refractive index with respect to its immersion medium as it thickens.

#### Ellipsometric Responses for Heat-Cured Coatings

Figure 3 shows typical ellipsometric responses for steel with either polybutadiene or an acrylic lacquer which have been heat-cured. Several factors should be considered initially using a steel specimen with a heat-cured acrylic coating as an example.

Although the acrylic coating material "A" used was the same as that used to generate figure 5, the heat treatment process undoubtedly modifies the

---

\*The exact nature of these species is under investigation.

final polymer structure. In addition, recent evidence points to a "zone" of iron ions in that portion of the heat-cured polymer nearest to the oxide layer [12]. Moreover, the oxide layer under the polymer thickens considerably during the curing process. Measurements in our laboratory by cathodic reduction of stripped specimens show typically a 14 nm film while an ordinary air-formed film will range between 2.5 to 3.5 nm. The utility of cathodic reduction to estimate oxide film thicknesses has been described previously [8].

In examining the general features of the  $\Delta$  and  $\Psi$  parameters in figure 7, we note that they move in opposition to each other throughout the experiment. The suggestion here is that the observed changes are due predominantly to alterations in the oxide layer and that changes in surface texture (roughening) are insignificant. This interpretation is supported by lack of evidence from potential cycling experiments [8] for surface roughening at the conclusion of these measurements.

A detailed interpretation of this type of curve must remain somewhat speculative until more evidence can be accumulated. In Region I, the initial increase in  $\Delta$  and decrease in  $\Psi$  at  $\sim 1800$  min indicate an oxide film thinning in the high pH environment estimated at  $\sim 5$  nm (total film  $\sim 14$  nm). Coating delamination probably occurs at this point, but the metal itself is still protected by  $\sim 9$  nm of film. Thus, metal dissolution leading to surface roughening does not occur.

The events beyond 2000 minutes are not well understood. The sharp rise of  $\Delta$  and decline in  $\Psi$  maximizing at  $\sim 2500$  min (Region II) is believed to arise from changes in the polymer near the interface. The subsequent reversal of  $\Delta$  and  $\Psi$  may be related to the precipitation process noted earlier for the room temperature cured systems. The substantial rise of  $\Delta$  and leveling of  $\Psi$  along

with the concomitant signal deteriorations in Region III (beyond 5300 min) may be related to the accumulation of a substantial liquid layer at the interface.

#### The Dissolution of Air-Formed Oxide Films on Iron

It is well known that air-formed oxide films on iron can be removed by cathodic reduction in borate buffer solutions at  $\sim$  pH 8.5. Results in our laboratories have shown that both air-formed and thermally grown films on iron and steel can also be dissolved in aerated saturated NaOH (pH > 14) at -1200 mV S.C.E.

Typical ellipsometric evidence for this process on uncoated iron is shown in figure 10. Note that when the cathodic potential is applied,  $\Delta$  and  $\Psi$  move in opposite directions as the film is removed. These observations are consistent with those mentioned earlier for coated specimens undergoing cathodic delamination, i.e., the presence of a highly alkaline environment promoting dissolution of the interfaced oxide film. Unfortunately, the potential at the coating/substrate interface is not known so that it is not possible, at present, to simulate the subcoating conditions exactly. However, these simulation experiments suggest that oxide film dissolution is a reasonable process to expect in cathodic regions.

#### The Development of Cathodic Areas

Since cathodic regions under coatings ultimately become the sites for coating delamination it is important to understand the development of these regions. The following experiments were designed to probe, in a preliminary fashion, the spatial disposition of cathodes in the vicinity of an active anode.

Polybutadiene on Steel: Figure 8 shows a study of PBD coated steel undergoing corrosion. The specimen was arranged to be translated  $\sim$  3 mm to

either side of a central position to observe the progress of subcoating events at different regions. In this manner, the experiment becomes a study in triplicate under identical conditions. The coating was damaged at the specimen center at  $\sim 1350$  min. It will be noted that significant changes in the ellipsometric  $\Delta$  and  $\Psi$  parameters occur first at the center "c" position. The general shape of the curves is similar to that for the heat-cured acrylic shown in figure 7. As mentioned previously, a detailed analysis of the ellipsometric responses for the heat-cured coating systems has not yet been possible. Again we propose that at least a part of the initial rise of  $\Delta$  and decline in  $\Psi$  is due to oxide film thinning. From this effect we infer that delamination has taken place. The first evidence for film thinning is manifested in the cathodic region immediately surrounding the induced anode. Further evidence for this activity gradually appears in regions "a" and "b," some 3 mm distant, on somewhat different time scales. An asymmetric development of the delamination process is apparent. While, as a first approximation, it can be proposed that the cathodic regions develop radially outward from the central anode. The possibility of cathodes developing and propagating remotely cannot be excluded. Thus, the asymmetry can arise from either a true preferred propagation of the delamination front from the central holiday towards region "a" or from the progress of a remote cathode in or near region "a." Evidence for the existence of remote cathodes has been obtained in experiments with a segmented substrate.

Segmented Fe Specimen with Acrylic Coating "A": In dealing with the corrosion of coated metal systems the location of the anodes is usually apparent. However, the location of cathodes which support these anodes is often more difficult to ascertain. Intuitively, one might expect cathodes to develop initially in the region immediately surrounding an anode. Our experiments with a coated,

segmented iron specimen indicate that the real time development of cathodes can be a relatively complex process.

Figure 9 shows the phase retardation ( $\Delta$ ) and pH data for the segmented iron sample. While the coating is intact during the first 1400 minutes,  $\Delta$  for both segments changes only slightly while the pH is erratic and ranges between 5 and 8. The coating on segment "a" is punctured at 1400 minutes, while that of segment "c" is left intact. If segments "a" and "c" are coupled electrically by joining the copper conductors attached to each, the pH on "c" rises to about 13.5 while the ellipsometric  $\Delta$  parameter for "c" is relatively constant. Delta for "a" shows the typical response described and interpreted earlier for this substrate-coating system (fig. 5) a brief rise followed by a substantial decline. If the conductors joining "a" and "c" are uncoupled, the subcoating pH drops to a value near 8 within a few minutes. Rejoining the conductors results in a subcoating pH reading of about 13 within 5 minutes. This process is quite reproducible and indicates that high subcoating levels of  $\text{OH}^-$  ions can only be maintained if their production rate exceeds their loss rate (probably by diffusion). However, if the segments are electrically coupled, for the next few days, the subcoating pH on "c" declines. Delta for "a" decreases markedly while  $\Delta$  for segment "c" also declines, but to a much lesser extent.

These responses are interpreted as follows: oxygen and water permeate the coating in some areas and reach the surfaces of "a" and "c" during the first 1400 minutes. Thus, two of the three components to effect the cathodic reduction of  $\text{O}_2$  are in position under the coating. Moreover, small quantities of adsorbed  $\text{O}_2$  and water were undoubtedly present on the surface before the coating was applied. When the coating on "a" is damaged, an anode develops rapidly at the puncture site and supplies the final component, electrons,

for  $O_2$  reduction. For "a" the electron flow is through the metal sector itself while for "c" the electrons must take the longer path through the coupled conductors. There is a net accumulation of product  $OH^-$  ions under the coating in both sectors. Initially the rate of the reduction reactions is probably limited by the rate of  $Na^+$  ion permeation [13] since these ions serve to transport charge through the coating and maintain electroneutrality with the subcoating  $OH^-$  ions. However, a second transport mechanism develops on "a" in the vicinity of the puncture. Oxygen, water, and  $Na^+$  ions start to migrate laterally and establish proximate cathodes surrounding the active anode [9]. As these proximate cathodes grow they gradually consume a larger portion of the anodically generated electrons. Eventually the remote cathodes on "c" are no longer needed and cease to function. Undoubtedly the presence of low resistance pathways within "a" and relatively higher resistive pathways between "a" and "c" contribute to the relative viability of these cathodic regions.

At the conclusion of the experiment the acrylic coating was stripped with toluene and each segment individually subjected to cathodic reduction in borate buffer solution. Segment "a" showed a net oxide film growth of 7.7 nm and evidence of surface roughening. Segment "c" showed a net oxide film growth of only 2.7 nm and little if any evidence of surface roughening. These results are consistent with the picture of extensive cathodic activity on "a" and limited cathodic activity on "c" provided by the ellipsometric responses [8].

### Summary

1. Iron and steel specimens with selected organic coatings bonded to their air-formed oxide films have been studied while undergoing corrosion. Ellipsometric evidence on these systems with room temperature cured coatings indicates that dissolution of the interfacial oxide film is the predominant mode of coating delamination.
2. Similar studies on systems where the coatings were heat cured, suggest that a similar delamination mechanism may apply. The complexities of a thickened interfacial oxide and probable modification of the polymer during the curing process have rendered the ellipsometric data difficult to fully interpret.
3. Air and thermally formed oxide films on iron and steel can be dissolved in strong NaOH solution at cathodic potentials. This observation supports the oxide dissolution mechanism proposed for cathodic delamination.
4. Ellipsometric experiments combined with subcoating pH measurements and specimen modifications have been utilized to probe the development of cathodic areas. The results suggest that remote cathodes are important during the early stages of corrosion but that proximate cathodes tend to dominate as corrosion progresses.

### Acknowledgments

The author is grateful to Dr. J. Kruger for many helpful discussions. This work was partially supported by the Office of Naval Research under contract No. NAONR 18-69.



## References

- [1] Henry Leidheiser, Jr., Ind. Eng. Chem. Product Research and Development, 20, 547 (1981).
- [2] Henry Leidheiser, Jr., and Martin Kendig, Corrosion, 32, 69 (1976).
- [3] W. Funke, Prog. Organic Coatings, 9, 29 (1981).
- [4] J. J. Ritter and M. J. Rodríguez, Corrosion, 38, 223 (1982).
- [5] J. C. Bolger and A. S. Michaels, Interface Conversion for Polymer Coatings, Weiss and Cheeves, Eds., Elsevier, New York (1968).
- [6] J. S. Hammond, J. W. Holubka, and R. A. Dickie, J. Coatings Technol., 51, 45 (1979).
- [7] E. L. Koehler, Corrosion Control by Organic Coatings, Henry Leidheiser, Jr., Ed., National Association of Corrosion Engineers, Houston, Texas (1981), p. 87.
- [8] J. J. Ritter and J. Kruger, Corrosion Control by Organic Coatings, Henry Leidheiser, Jr., Ed., ibid., p. 28.
- [9] Henry Leidheiser, Jr., Wendy Wang, and Lars Igetoft, Progr. in Organic Coatings (1982), to be published.
- [10] J. J. Ritter and J. Kruger, Surface Science, 96, 364 (1980).
- [11] P. K. Schenck and J. J. Ritter, to be published.
- [12] J. Castle, private communication.
- [13] H. Leidheiser, Jr., and W. Wang, Corrosion Control by Organic Coatings, Henry Leidheiser, Jr., Ed., NACE, Houston, Texas (1981), p. 74.

### Figure Captions

1. Drawing showing the relationships of components for the segmented specimen. "a" and "c" are sections of iron formed by dividing an iron cylinder along its altitude and diameter.
2. Plots of phase retardation ( $\Delta$ ) vs time for three iron/coating systems undergoing corrosion in a dilute chloride medium. The coatings were cured in air at room temperatures.
3. Plots of phase retardation ( $\Delta$ ) vs time for two steel/coating systems undergoing corrosion in a dilute chloride medium. The coatings were cured in air at 200 °C.
4. ( $\Delta$ ) and ( $\Psi$ ) plotted vs time for the iron/collodion system undergoing corrosion in 0.05M NaCl.
5. ( $\Delta$ ) and ( $\Psi$ ) plotted vs time for the iron/acrylic "A" system undergoing corrosion in 0.05M NaCl.
6. ( $\Delta$ ) and ( $\Psi$ ) plotted vs time for the iron/acrylic "B" system undergoing corrosion in 0.05M NaCl.
7. ( $\Delta$ ) and ( $\Psi$ ) plotted vs time for the steel/acrylic "A" system undergoing corrosion in 0.05M NaCl. Acrylic "A" was heat-cured.
8. Phase retardation ( $\Delta$ ) and amplitude attenuation ( $\Psi$ ) plotted vs time for the steel/polybutadiene system undergoing corrosion in 0.05M NaCl. The coating was heat-cured. The open ellipses shown in the inset indicate the three regions on the specimen face where ellipsometric measurements were made. The curves are labeled corresponding "a," "b," and "c."
9.  $\Delta$ ,  $\Psi$ , and pH plotted vs time for the segmented iron/acrylic "A" system in 0.05M NaCl. Inset shows a facial view of the specimen and open ellipses indicate regions studied ellipsometrically.

10.  $\Delta$ ,  $\Psi$ , and  $V$  plotted vs time for uncoated iron in saturated NaOH. Changes in  $\Delta$  and  $\Psi$  when potential is lowered to -1200 mV indicate the dissolution of the air-formed oxide film.

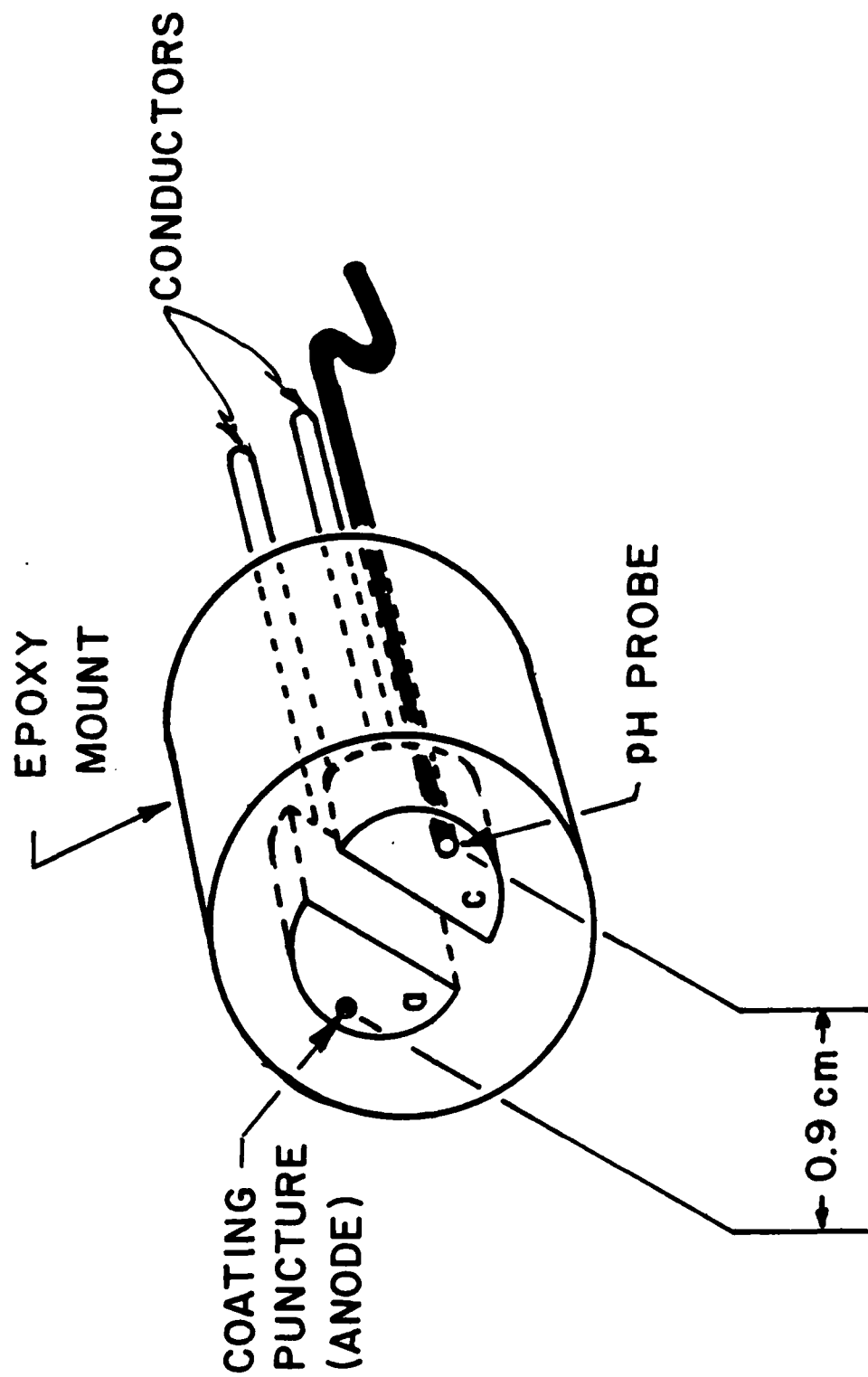


Figure 1

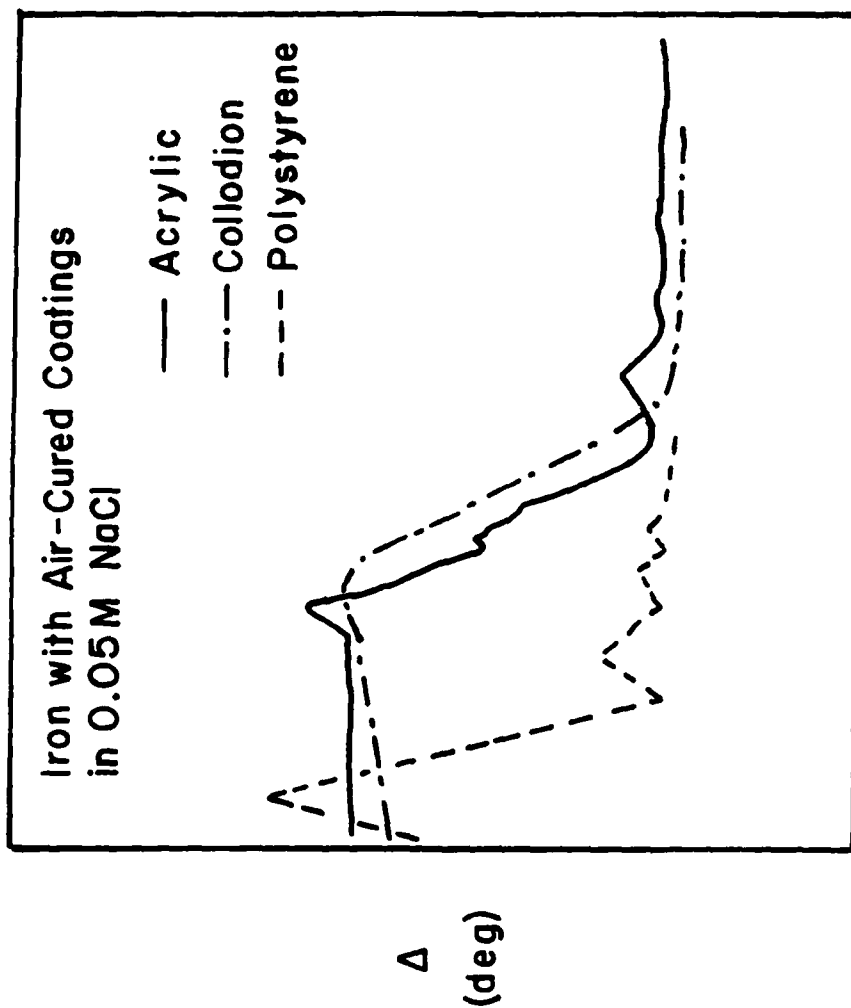


Figure 2

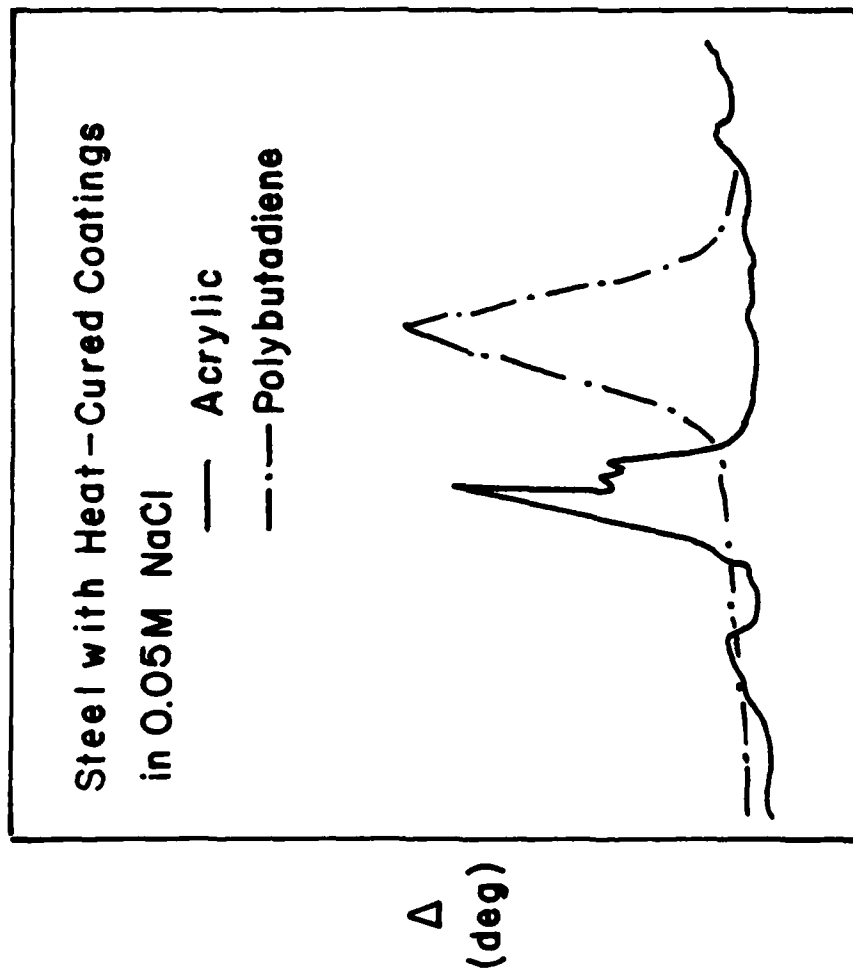


Figure 3

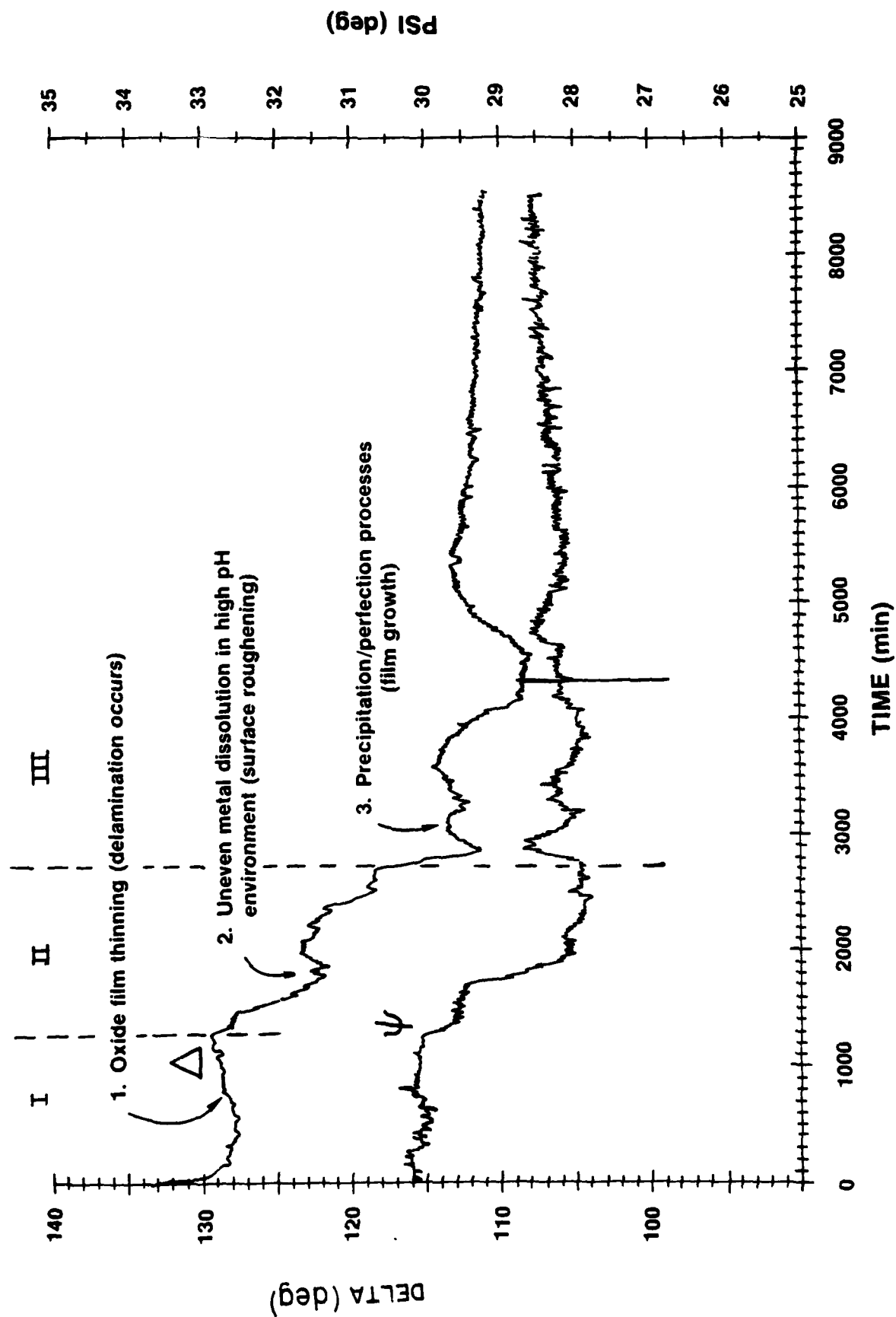


Figure 4

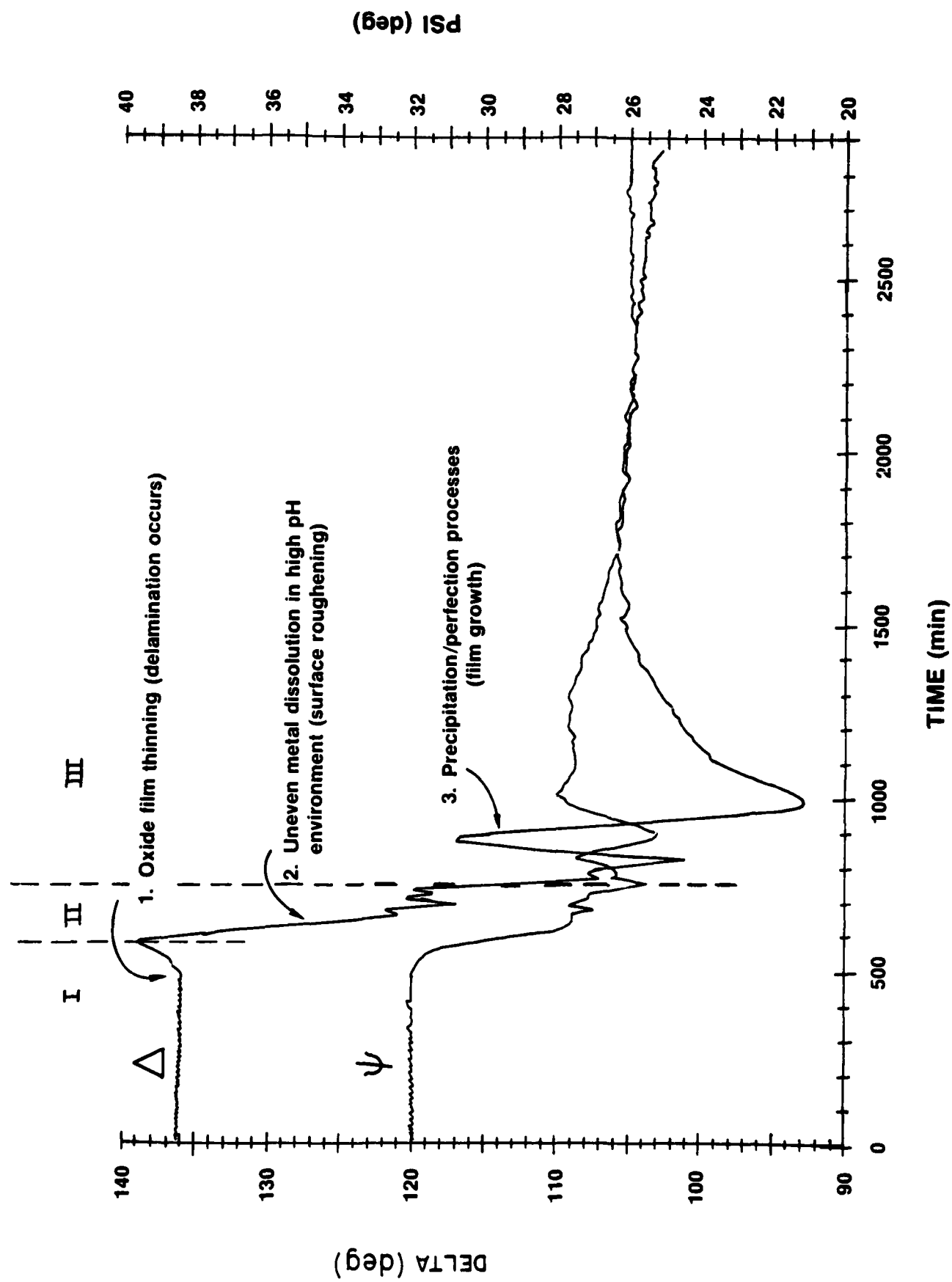


Figure 5



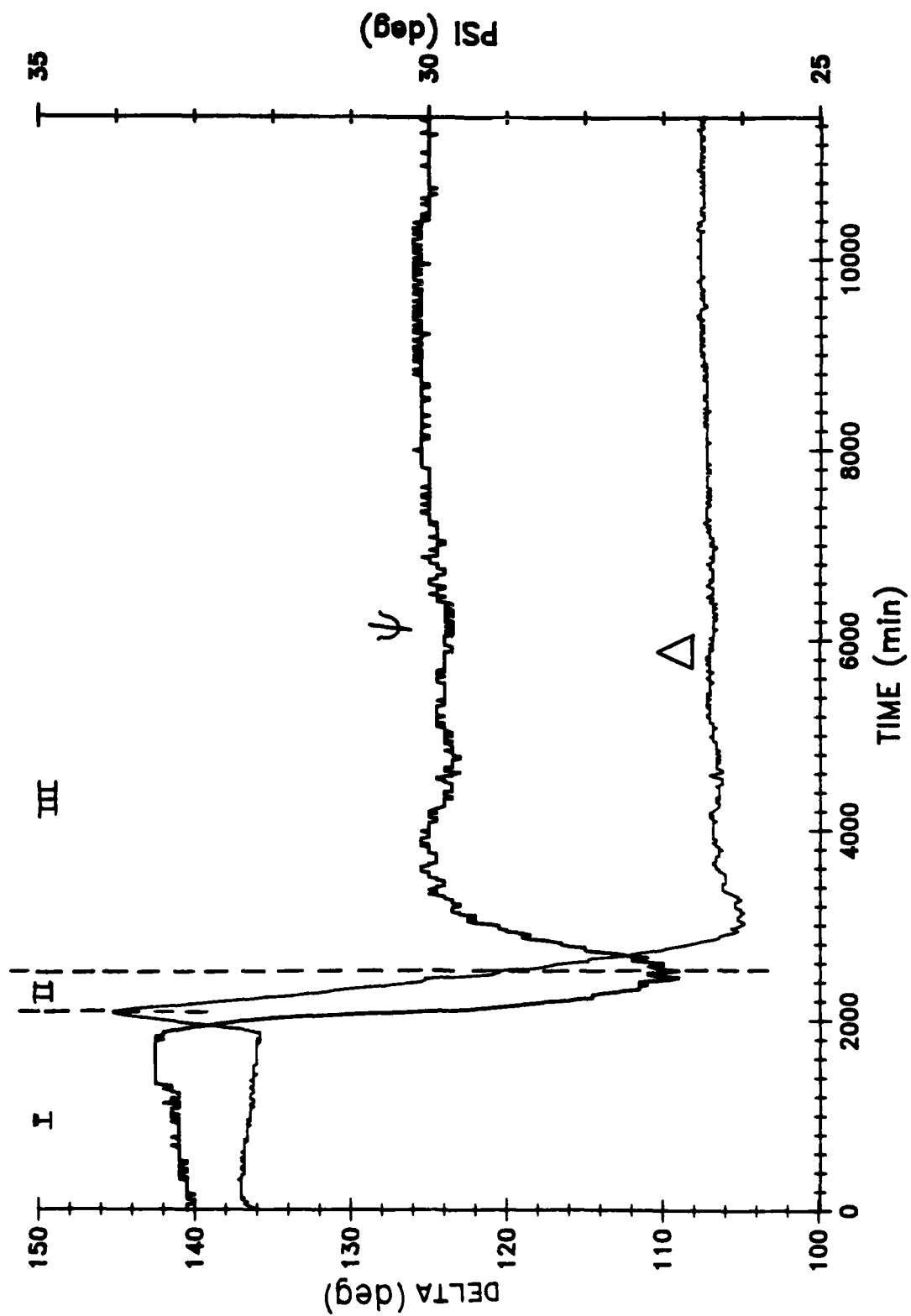


Figure 6

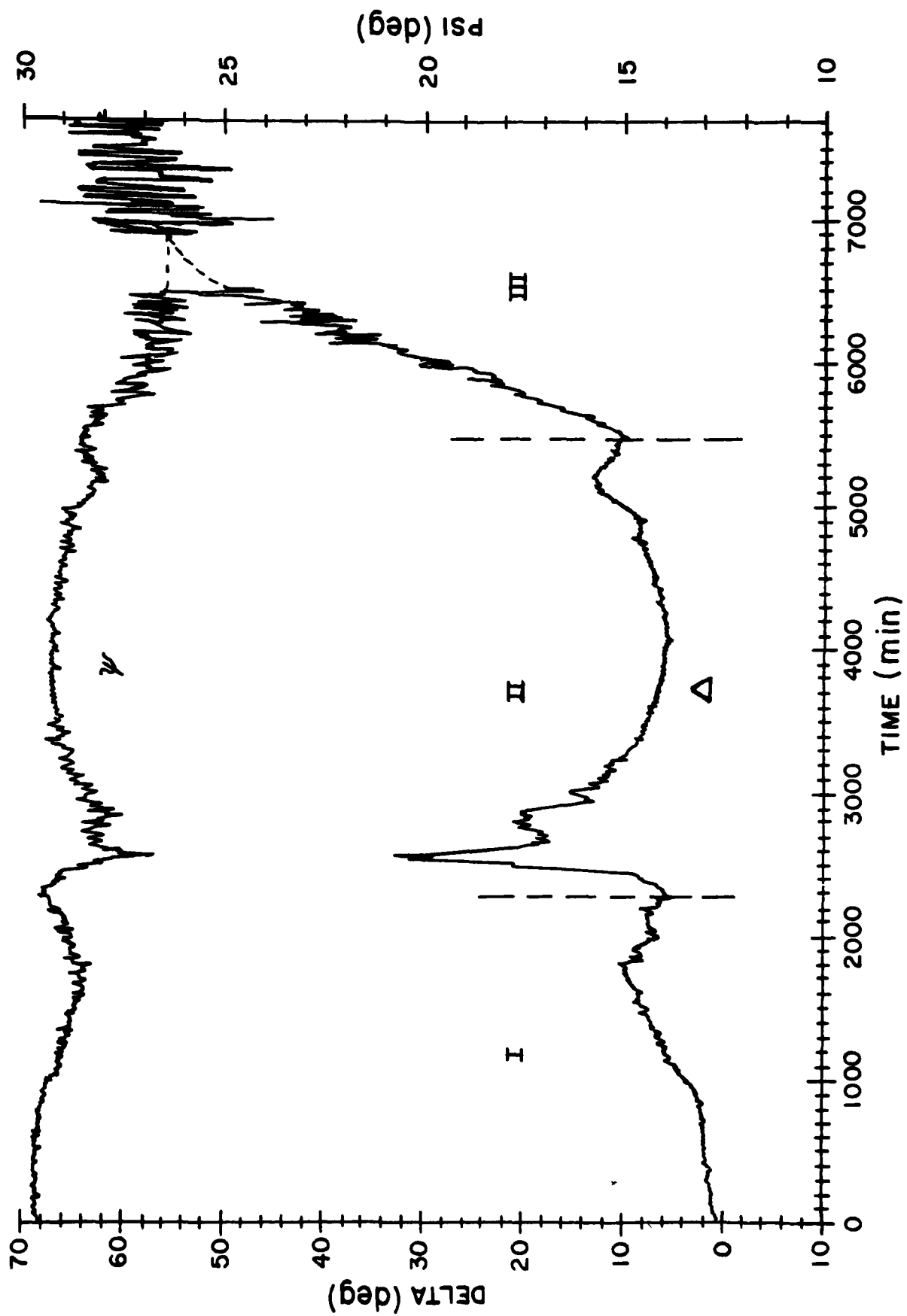


Figure 7

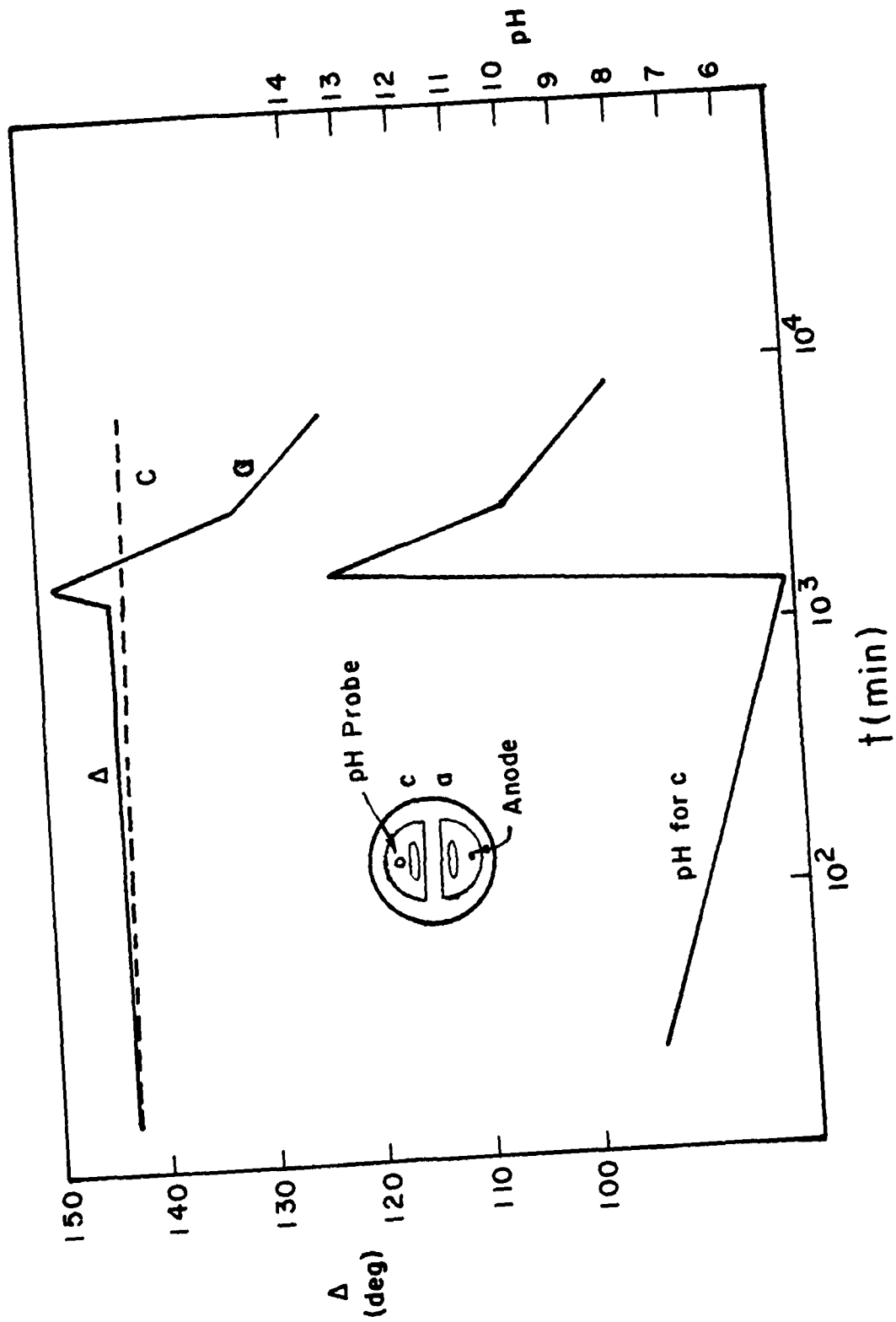


Figure 8

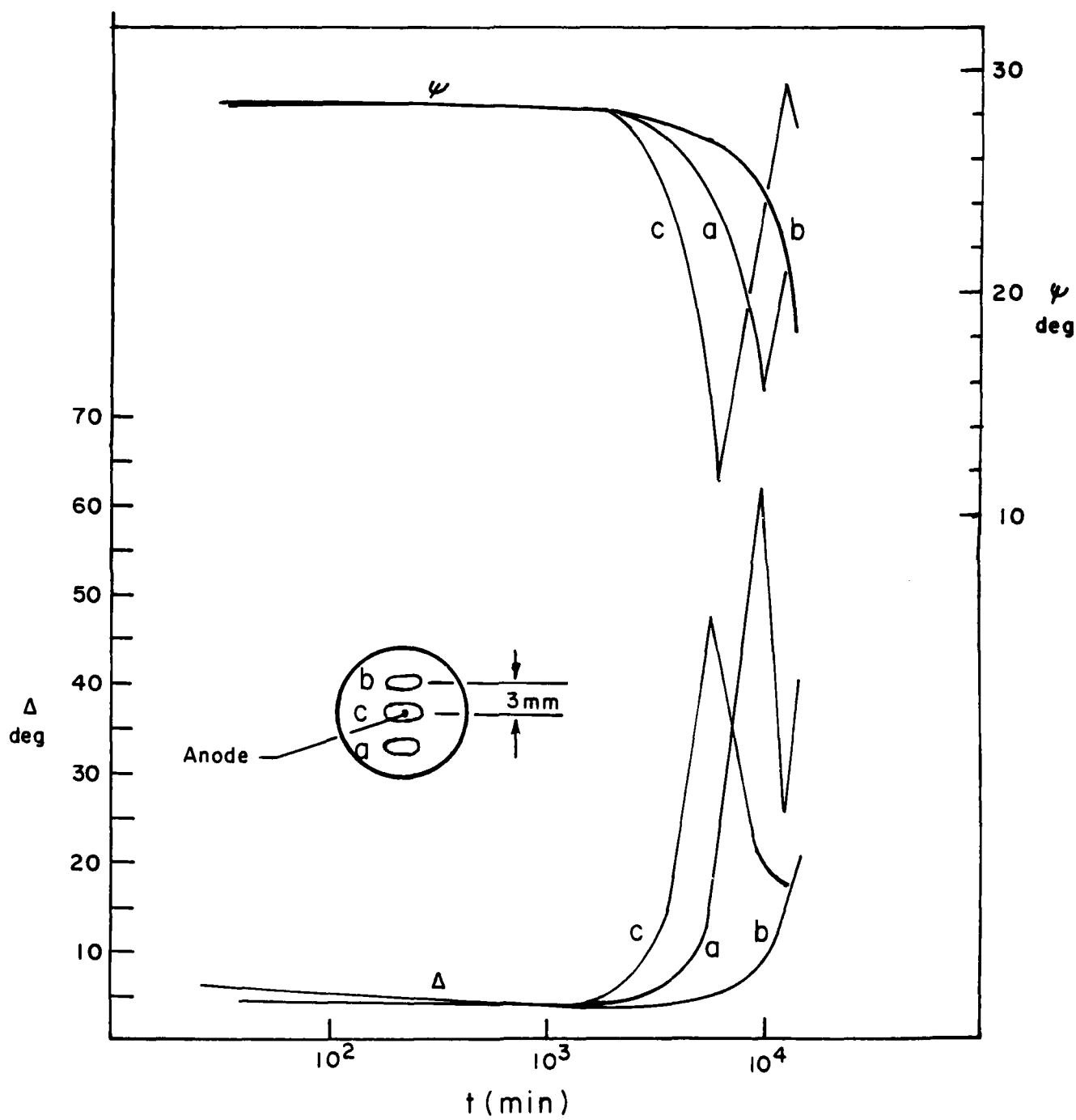


Figure 9

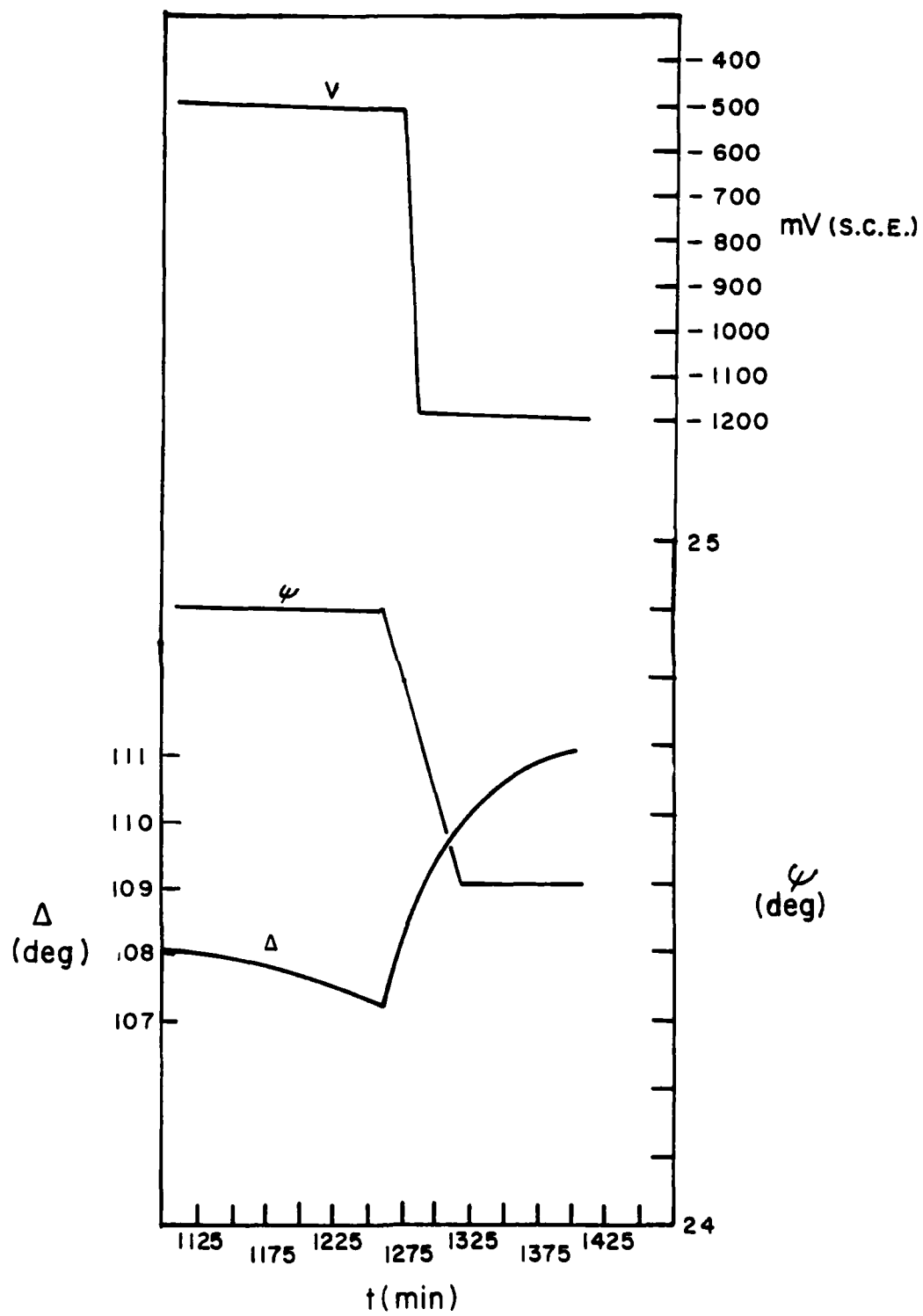


Figure 10

PART II. To be published in Proceedings of Eighth International Conference in Organic Coatings Science and Technology, Athens, Greece, 12 July-16 July 1982, in the series Advances in Organic Coatings Science and Technology.

A NEW TECHNIQUE TO STUDY CORROSION MECHANISMS UNDER ORGANIC COATINGS

J. J. Ritter and J. Kruger  
Materials Chemistry Division  
National Bureau of Standards  
Washington, D.C. 20234 USA

ABSTRACT

Transparent organic coatings on iron are used to simulate painted metal surfaces for simultaneous ellipsometric and electrochemical measurements. These studies show that significant changes occur both in the metal oxide film and in the subcoating environment during prolonged immersion in dilute  $\text{Cl}^-$  media. The relationship of these changes to aspects such as metal passivation, surface roughening, coating delamination, type of coatings, and inhibitor behavior are discussed.

Key words: Corrosion; electrochemistry; ellipsometry; iron; organic coatings; oxide films; passivation; pH

## A NEW TECHNIQUE TO STUDY CORROSION MECHANISMS UNDER ORGANIC COATINGS

J. J. Ritter and J. Kruger  
Materials Chemistry Division  
National Bureau of Standards  
Washington, D.C. 20234, USA

There exists a great need for in situ techniques that are capable of studying the growth and dissolution of oxide films and other films that exist on a painted metal surface exposed to a corrosive aqueous environment. Also of great value would be a technique that could detect changes in the organic coating (paint), changes in the environment that develop under the coating, and finally how such changes lead to the delamination processes, i.e., the detachment of a paint from an oxide-covered metal surface.

Recent work [1,2] from this laboratory has described such a technique, a combined ellipsometric-electrochemical technique, that is capable of in situ studies of the fundamental corrosion processes occurring on a metal surface under an organic coating. This paper reviews the past work and extends it to an exploration of the role played by the type of organic coating in affecting the processes that occur at the metal-coating interface.

### Description of the Ellipsometric-Electrochemical Technique

A detailed description of the technique is given elsewhere [1]. In brief, a coated metal is experimentally modeled by coating a polished iron specimen with a transparent organic coating. In the early experiments cellulose nitrate (collodion) coatings were used because such a coating permits rapid initiation of the corrosion processes. A transparent coating is necessary for ellipsometric measurements to be made. A miniature pH probe is inserted through a hole in the back of the specimen. The tip of

this probe is made flush with the surface of the specimen after the specimen is coated with a transparent organic coating. Thus, it is possible to make pH measurements under the coating while also making ellipsometric measurements by passing elliptically polarized light through the coating and reflecting it from the polished metal surface (see fig. 1). Previous studies [1] showed that the ellipsometric parameters  $\Delta$ , the relative phase retardation, and  $\psi$ , the relative amplitude reduction, are most sensitive to changes at the metal-metal oxide interface under an organic coating, all immersed in an aqueous solution. It is thus feasible to relate, for example, the parameter  $\Delta$  to the growth or dissolution of the oxide film at the surface of the metal and under the organic coating, while simultaneously measuring the pH of the micro-environment that develops between the coating and the metal specimen.

It is possible to apply this technique to study coatings containing corrosion inhibitory pigments which are incorporated in the organic coating or placed on the metal surface in a way that does not interfere with the ellipsometric measurements. Because of the complexity of the multi-layered systems involved, the ellipsometric measurements are used in a mainly qualitative way. This means that times and extents of changes are measured rather than exact film thicknesses and film optical parameters. To help in the interpretation of the optical results, cathodic reduction experiments are also carried out on iron surfaces from which the organic coating has been stripped. By this means a semi-quantitative measurement of oxide film thickness can be made and related to the ellipsometric parameters which are measured prior to the stripping of the coating on the iron. Specifically, the extent of oxide film growth under the coatings is estimated at the conclusion of an experiment by stripping the coating with methanol, and



cathodically reducing the metal surface at -1000 mV S.C.E. in deaerated borate buffer solutions (pH 8.5) while observing the surface with the ellipsometer. Oxide film thicknesses are calculated assuming that the film is essentially  $\text{Fe}_2\text{O}_3$  and that each degree change in  $\Delta$  corresponds to 0.6 nm of film. The details of the technique are shown schematically in fig. 2.

The presence of surface roughness is qualitatively detected by cycling the specimen potential between -1000 and +200 mV approximately 60 times. In our experience a significant increase in the  $\Delta$  parameter indicates surface smoothing as a result of electrochemical polishing [2].

Contributions from the coating to changes in  $\Delta$  are estimated by ellipsometrically monitoring collodion coated gold specimens in 0.05 N NaCl and in saturated NaOH (pH  $\sim$  15).

The materials and specimen preparation details for the experiments to be described are as follows:

The iron specimens were cast in epoxy, polished to a 0.05  $\mu\text{m}$  finish and dipped in a 1:1 collodion-methanol mixture (1 gm of a proprietary acrylic in 6 ml toluene and 100 mg polystyrene in 1.5 ml toluene when these coating materials were studied) to give a coating of from 10 to 30  $\mu\text{m}$  in thickness over the face of both the metal and the epoxy mount. The prepared specimen mounted as shown in fig. 1 was placed in a polytetrafluoroethylene lined cell which was filled with 0.05 N NaCl. Inhibitor materials were either applied directly to the metal before coating or dispersed as a finely ground powder in the collodion-methanol mixture. For the case of  $\text{SrCrO}_4$ , the metal specimen was dip coated, finely powdered  $\text{SrCrO}_4$  applied to the surface of the semi-cured coating, and a second coat applied to cover the inhibitor.

A phosphate-chromate surface treatment was accomplished as follows:

Solution I:  $\text{H}_3\text{PO}_4$  3.0 g,  $\text{ZnO}$  1.5 g,  $\text{NaNO}_3$  1.0 g, make up with  $\text{H}_2\text{O}$  to 100 ml.

Solution II:  $\text{K}_2\text{Cr}_2\text{O}_7$  0.7 g,  $\text{H}_3\text{PO}_4$  0.5 g, make up with  $\text{H}_2\text{O}$  to 100 ml.

The solutions were used at room temperature. The face of the specimen was rotated in a horizontal plane at 50 rpm in a mixture comprised of 8 ml of solution I and 2 ml of solution II for a period of six minutes. This procedure gave a homogeneous surface finish which retained sufficient specular quality to allow ellipsometric measurements.

#### Prototype Coating (Collodion) Studies

The ellipsometric measurements on collodion-coated iron specimens showed changes in both the  $\Delta$  and  $\psi$  parameters with time (see fig. 3). By far the largest change was seen in the  $\Delta$  parameter which always showed a decrease. It is known that several factors could contribute to this directional change in  $\Delta$ , among them, metal oxide film growth, surface roughening [3], and possibly coating deterioration.

At least two stages can be discerned in fig. 2. During the first stage (generally up to around 1000 mm) a gradual rise in pH was observed, accompanied by an increase of several degrees in  $\Delta$ . This increase in  $\Delta$  was not always observed and its origin is not readily explained by the ellipsometric modeling calculations. The second stage started when the pH approached 11 and the  $\Delta$  values began to decrease significantly. Accompanying the onset of the second stage was the invariable appearance of small anodic regions (sites where rust was observed). The overall anodic to cathodic (bright uncorroded) area ratios ranged from 1/30 to 1/600. The pH remained high during the third stage, where fig. 2 shows that fluctuations in  $\Delta$  were observed.

The most significant change occurs in the  $\Delta$  parameter during the second stage. This change arises from three factors given below along with their

estimated contributions to the overall  $\delta\Delta$ : (a) metal surface roughening,  $\sim 55$  percent; (b) oxide film growth,  $\sim 35$  percent, and (c) changes in coating material in a high pH environment,  $\sim 10$  percent. It will be noted that the second stage changes of  $\Delta$  with time appear to approximate a semi-logarithmic relationship, i.e.,  $\Delta = k \log t + c$ . This law is frequently observed in the growth of passive films on metals [4].

Using the stripping-cathodic reduction technique described earlier, experiments on uncoated iron in solutions simulating the undercoating environment and microanalytical measurements of the subcoating environment, a reasonable interpretation of the three stages identified by the ellipsometric measurements can be made as follows:

First stage: During the first stage, oxygen, water,  $\text{Na}^+$ , and  $\text{Cl}^-$  permeate the coating. The dilute  $\text{Cl}^-$  solution that develops under the coating promotes the pitting of the pre-existing air-formed oxide film on the iron surface. The pit sites become anodes where ferrous ions go into solution, the rest of the iron surface becomes progressively cathodic and supports the reduction of  $\text{O}_2$ . The production of  $\text{OH}^-$  leads to the rise in pH.

Second stage: When the pH reaches values as high as about 15, this stage commences with a sharp drop in  $\Delta$ -values. Studies of uncoated iron in saturated sodium hydroxide solutions (pH  $\sim 15$ ), a solution that simulates the second stage subcoating environment, suggest that the potential at the onset of the second stage can vary from -900 to -150 mV SHE (see fig. 4). The Pourbaix potential pH diagram [5] indicates that at the negative end of this potential range iron can go into solution as  $\text{HFeO}_2^-$  or  $\text{FeO}_4^{2-}$  ions. At the positive end  $\text{HFeO}_2^-$  can oxidize forming a solid corrosion product film,  $\text{Fe}_2\text{O}_3$ . Experiments involving the cathodic reduction of iron surfaces

from which the organic coating was stripped during stage two indicated that both surface roughening (presumably resulting from the dissolution of the iron to produce  $\text{HFeO}_2^-$  and/or  $\text{FeO}_4^{2-}$ ) and oxide film growth occur during this stage and are primarily responsible for the decrease in the values of  $\Delta$  in the manner shown in fig. 4 for the simulated environment. Thus the high pH environment and concomitant decreases in  $\Delta$ -values occur only when active corrosion is underway somewhere on the surface of the coated metal. Our technique provides an in situ way to detect the presence of serious subcoating corrosion and to measure the overall kinetics for some of the subcoating processes.

What are the implications of the corrosion processes just suggested for stage two for coating failure mechanisms? Speculating, one might envision that, while the coating is still intact, the initial formation of small "two dimensional" localized corrosion cells that develop with permeation of the coating by  $\text{H}_2\text{O}$ ,  $\text{O}_2$ ,  $\text{Cl}^-$ , and  $\text{Na}^+$ . This activity will proceed rapidly at porous or thin portions of the coating. These cells could be the starting sites for corrosion. Ritter and Rodriguez [5] have recently carried out microanalytical determinations of the concentration build-up of  $\text{Cl}^-$  in the subcoating environment and used that information to propose a picture of the processes that lead to this delamination. The picture that they have developed is shown in fig. 5. This view describes how, following the build up of  $\text{Cl}^-$  concentration and the development of separated anodic and cathodic sites as a result of the chemical reactions shown in fig. 5a, a "breakthrough" can occur between these separated sites (fig. 5b) during delamination, causing the mixing of the acidic anodic sites with the alkaline cathodic sites. Figure 6 from the Ritter and Rodriguez paper shows experimental evidence for this "breakthrough," the detection of a large drop in pH.

Such a delamination and breakthrough process as a result of the anodic and cathodic reactions shown in fig. 5a continue to promote the enlargement of the delaminated regions that are observed during stage two.

Third stage: Experiments with collodion coated gold in a high pH ( $\sim 15$ ) solution indicate organic coating deterioration after prolonged exposure. This deterioration may be partially responsible for the erratic fluctuations of  $\Delta$  that constitute the third stage.

#### Effect of Inhibitory Pigments

When a corrosion inhibitory pigment or pigment-like compound such as  $K_2CrO_4$  was incorporated into the collodion coating as small "islands" surrounding the area observed with the ellipsometer, results similar to those shown in fig. 7 were observed. The first stage was longer, the second stage involved a much slower decrease in  $\Delta$ -values, as compared to a non-inhibited coating, and the third stage was absent. Also, the increase in pH was less, usually remaining below pH 10.

Table I lists the rate constants,  $k$ , for the decrease in  $\Delta$  in the second stage for coated iron with various applications of different inhibitory pigments.

With reference to Table I it is readily seen that the rate of ellipsometrically observed subcoating events for coated iron and for coated iron which had been given a phosphate-chromate pretreatment were quite comparable. However, when  $K_2CrO_4$  was present at the metal surface, the rate was slower by a factor of 10, whereas  $ZnCrO_4$  applied in a similar fashion slowed the rate by only a factor of two. This phenomenon may be partly related to solubility differences between the two inhibitors. Inhibitors dispersed throughout the coating gave a similar factor of two reduction in the rate. The mechanism by which chromates inhibit corrosion reportedly involved the

incorporation of chromium into an existing oxide film, i.e., a chemical and structural modification of the existing oxide film which resulted in improved protection [6]. The rate constants derived from the present work seem to be related to inhibitor ion mobilities and accessibilities to the substrate surface. Contributions to the  $\Delta$  parameter due to modifications of the metal oxide (e.g., upon the incorporation of chromium) which may change its refractive index, are expected to be small for films  $< 5$  nm in thickness [7]. Thus, the thickness of these modified films could be estimated with reasonable confidence using parameters for  $\text{Fe}_2\text{O}_3$ .

Preliminary results from uncoated iron in a simulated subcoating environment of pH 15 (sat'd NaOH), 0.05 M  $\text{K}_2\text{CrO}_4$  and 0.05 M NaCl showed a change in  $\Delta$  of which approximately one-third was due to oxide film growth and the remainder ascribed to surface roughening. The oxide film growth on uncoated Fe even in this highly alkaline environment was only 2.4 nm as compared to the typical 6 nm growth measured for coated iron in the absence of inhibitor.

#### Effect of Type of Organic Coating

All of the experiments thus far described were carried out using a cellulose nitrate (collodion) coating. In this section, experiments will be described that show that the ellipsometric measurements can identify different processes leading to coating failure that depend on the type of organic coating used. Figure 8 shows three different types of ellipsometric results that are characteristic of different organic coatings. Figure 8a shows the behavior previously described for a room temperature air-cured collodion coating, an identical behavior for a room temperature air-cured polystyrene coating. If the collodion was replaced by a proprietary acrylic coating also room-temperature air-cured, the behavior observed was similar except for

a small difference observed during the first stage where no change in  $\Delta$  was observed until the acrylic coating was purposely punctured. Shortly thereafter  $\Delta$  rose sharply indicating perhaps a dissolution of the native oxide film under the coating followed by stage two where the surface roughening and oxide film regrowth, described earlier for the collodion coatings, was observed.

Rather pronounced differences in behavior were found for acrylic on iron or polybutadiene coatings on steel that were air-cured at a temperature considerably above room temperature (200 °C). This behavior can be seen in fig. 8c. First, the  $\Delta$  values in stage one were considerably lower than the air-cured cases. This was due to the existence of a 10 to 14 nm oxide film that formed under the organic coating during a 40-minute 200 °C curing process. Separate experiments holding an uncoated steel surface at the curing conditions verified the corresponding decrease in  $\Delta$ -values and the formation of the 10 to 14 nm oxide film. As fig. 8c shows, the low  $\Delta$ -values remained constant until the cured coatings were punctured, at which time the  $\Delta$ -values increased to a much greater extent than that observed during stage one for the acrylic (fig. 8b). This total increase in  $\Delta$  could not be accounted for by assuming it to be only the result of the dissolution of the thick oxide film formed during the curing process. It was estimated that only about one-half of the changes in  $\Delta$ -values were possibly caused by oxide dissolution. The origin of the rest of the increase in  $\Delta$  is not known. However, calculations aimed at relating the changes in the ellipsometric parameters,  $\Delta$  and  $\psi$  to changes in the optical constants of the polymeric coatings suggest that it is possible to model the optical changes observed if one assumes a decrease in refractive index in a 50 to 100 nm region of the coatings next to the metal oxide surface. Such a decrease in refractive

index (or density) of the polymer next to the metal could come about as a result of the dissolution of the oxide causing a destruction of the polymer-oxide bonds followed by as yet unexplained events responsible for the reduction of density in the interface region. This suggestion is a preliminary one and highly speculative. More work is needed to put such an interpretation of stage one events on firmer ground. Stage two appears to follow the same behavior as that observed for the coatings described in figs. 8a and 8b.

#### Summary and Conclusions

(1) The ellipsometric-electrochemical technique has shown that during the failure of an organic coating in an aqueous chloride environment oxide film and surface roughening take place on those areas of metal surface which are subjected to a highly alkaline environment.

(2) The results obtained suggest that the initial changes in the topography and possibly in the composition of the metal surface may be, at least, partially responsible for coating delamination.

(3) Inhibitory pigments retard active dissolution of iron and thereby suppress  $\text{OH}^-$  build-up which slows down oxide film growth and metal surface roughening. Use of the ellipsometric-electrochemical technique to follow such changes may be a valuable way to evaluate inhibitory pigment performance.

(4) The ellipsometric-electrochemical technique can detect differences in organic coating behavior; for example, high temperature cured coatings show much larger increases in  $\Delta$ -values during stage one as compared to room temperature coatings.

#### Acknowledgment

We are grateful to the Office of Naval Research which supported this work under NAONR 18-69 NRO 36-082.



## References

- [1] J. J. Ritter and J. Kruger, Surf. Sci., 96, 364 (1980).
- [2] J. J. Ritter and J. Kruger, in H. Leidheiser (Ed.), Corrosion Control by Organic Coatings, N.A.C.E., Houston, 1981, p. 28.
- [3] J. Kruger, Corrosion 22, 88 (1966).
- [4] F. P. Fehlner and N. F. Mott, Oxid. Met., 2, 59 (1970).
- [5] J. J. Ritter and M. J. Rodriguez, Corrosion, in press.
- [6] J. E. O. Mayne and M. J. Pryor, J. Chem. Soc., 1949, 1831 (1949).
- [7] J. Kruger, in R. H. Muller (Ed.), Advances in Electrochemistry and Electrochemical Engineering, Vol. 9, J. Wiley and Sons, New York, 1973, p. 250.

### Figure Captions

- Fig. 1. Details of the mounted iron specimen.
- Fig. 2.  $\Delta$ , relative phase retardation,  $\psi$  relative amplitude reduction, pH and  $\phi_{Fe}$ , potential of the iron surface versus standard hydrogen electrode (SHE) versus time for Fe with collodion in 0.05 N NaCl.
- Fig. 3. Schematic drawing showing changes in  $\Delta$  values during three steps in the film stripping-cathodic reduction procedure for measuring the film growth and surface roughening that occurs on iron surfaces under organic coatings after exposure to aqueous chloride environments.
- Fig. 4. Changes in  $\Delta$ ,  $\psi$ , and  $\phi_{Fe}$  (potential of iron surface vs SHE) of an iron surface in a saturated NaOH solution (pH 15).
- Fig. 5. (a) A summary of the equations proposed by Ritter and Rodriguez [5] for subcoating events leading to surface roughening, oxide film thickening, and the building up of  $Cl^-$  concentration.  
(b) Schematic diagram showing  $Cl^-$  ion entry into the hollow cone of anodic corrosion products in the presence of a remote cathode.  
(c) Schematic diagram suggesting one mode of "breakthrough" between anodic and cathodic areas. From Ref. 5.
- Fig. 6. Experimental curve showing changes in  $\Delta$  and pH as the corrosion process under an organic coating proceeds. The steady decrease in pH after 1200 min indicates a "breakthrough" between anodic and cathodic areas in the vicinity of the micro pH electrode. From Ref. 5.
- Fig. 7.  $\Delta$ ,  $\psi$ , pH, and  $\phi_{Fe}$  versus time for Fe with collodion and  $K_2CrO_4$  islands in 0.05 N NaCl.

Fig. 8. A comparison of ellipsometric ( $\Delta$  vs  $\log$  time) results for iron coated with (a) collodion or polystyrene, room temperature air cure, (b) acrylic, room temperature air cure, and (c) steel coated with polybutadiene or acrylic cured at 200 °C for 40 min in air.

Table I. Stage II Rate Constants for Ellipsometrically Measured Subcoating Events on Collodion-Coated Iron in 0.05 N NaCl

Summary of Ellipsometric Rate Constants for Stage II Events

Semi-Logarithmic Behavior Assumed  
 $d\Delta = k \log t + c$

<u>Specimen</u>	<u>Immersion Medium</u>	<u>k(deg)</u>
Uncoated Fe	Sat'd NaOH	76
Coated Fe	0.05 M NaCl	83
Coated Fe with deliberate holiday	"	73
Coated Fe with phosphate-chromate surface pretreatment	"	76
Coated Fe with K <sub>2</sub> CrO <sub>4</sub> "islands"	"	8
Coated Fe with ZnCrO <sub>4</sub> "islands"	"	35
Coated Fe with ZTOC* dispersed in coating	"	58
Coated Fe with K <sub>2</sub> CrO <sub>4</sub> dispersed in coating	"	42
Coated Fe with SrCrO <sub>4</sub> located between two layers of collodion	"	56

---

\*Zinc tetraoxochromate  
 $[Zn(OH)_2]_4 \cdot ZnCrO_4$

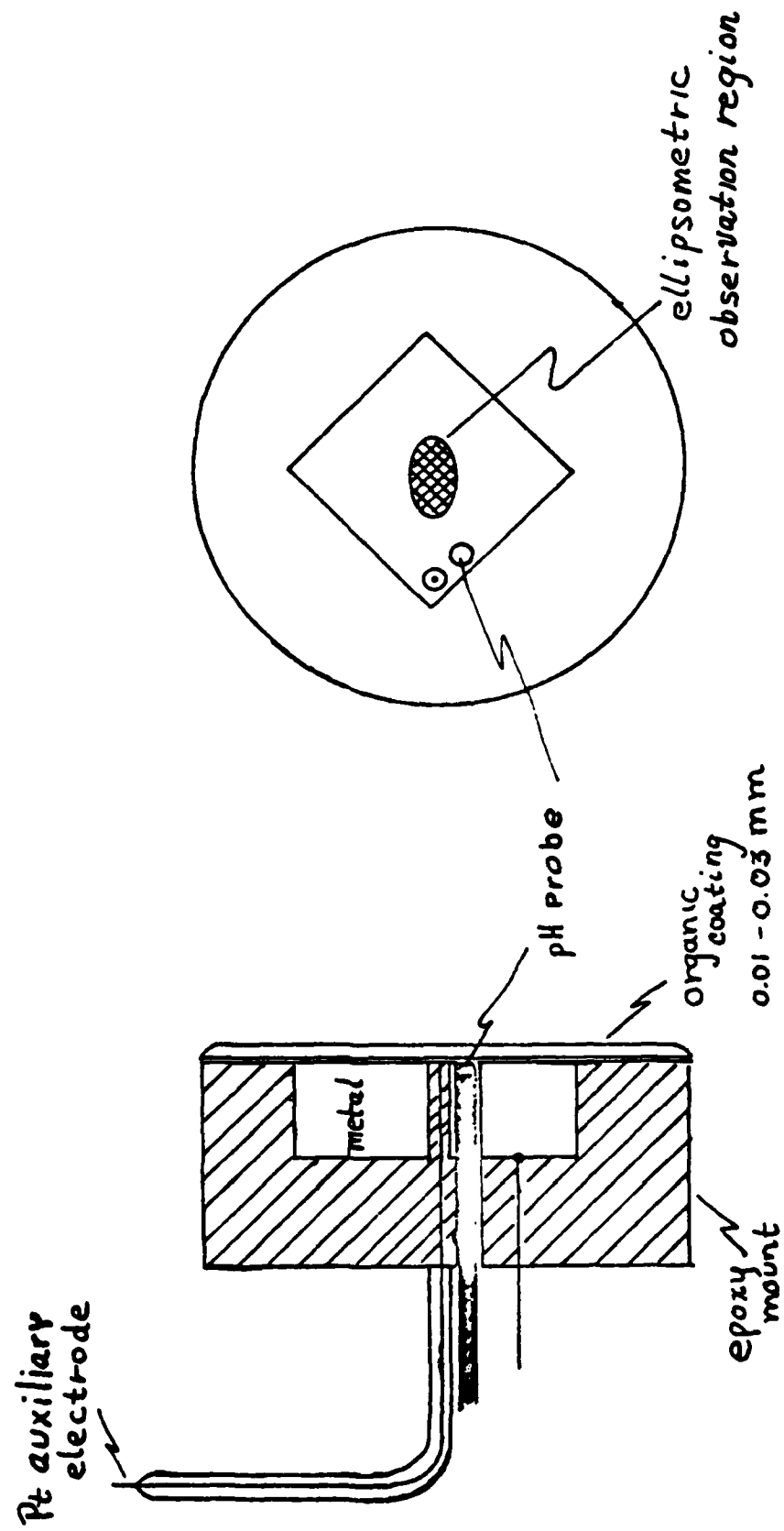


Figure 1

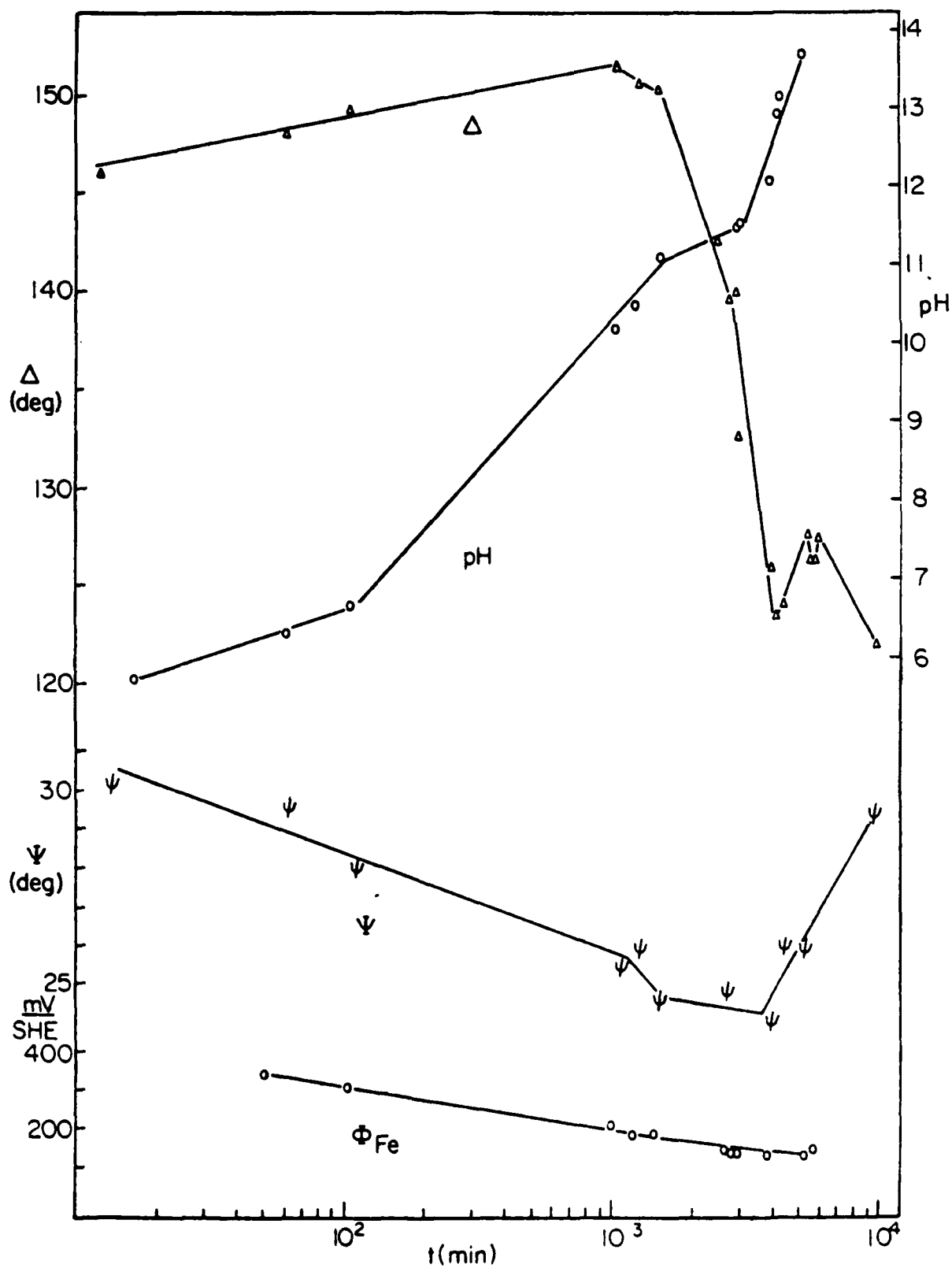


Figure 2

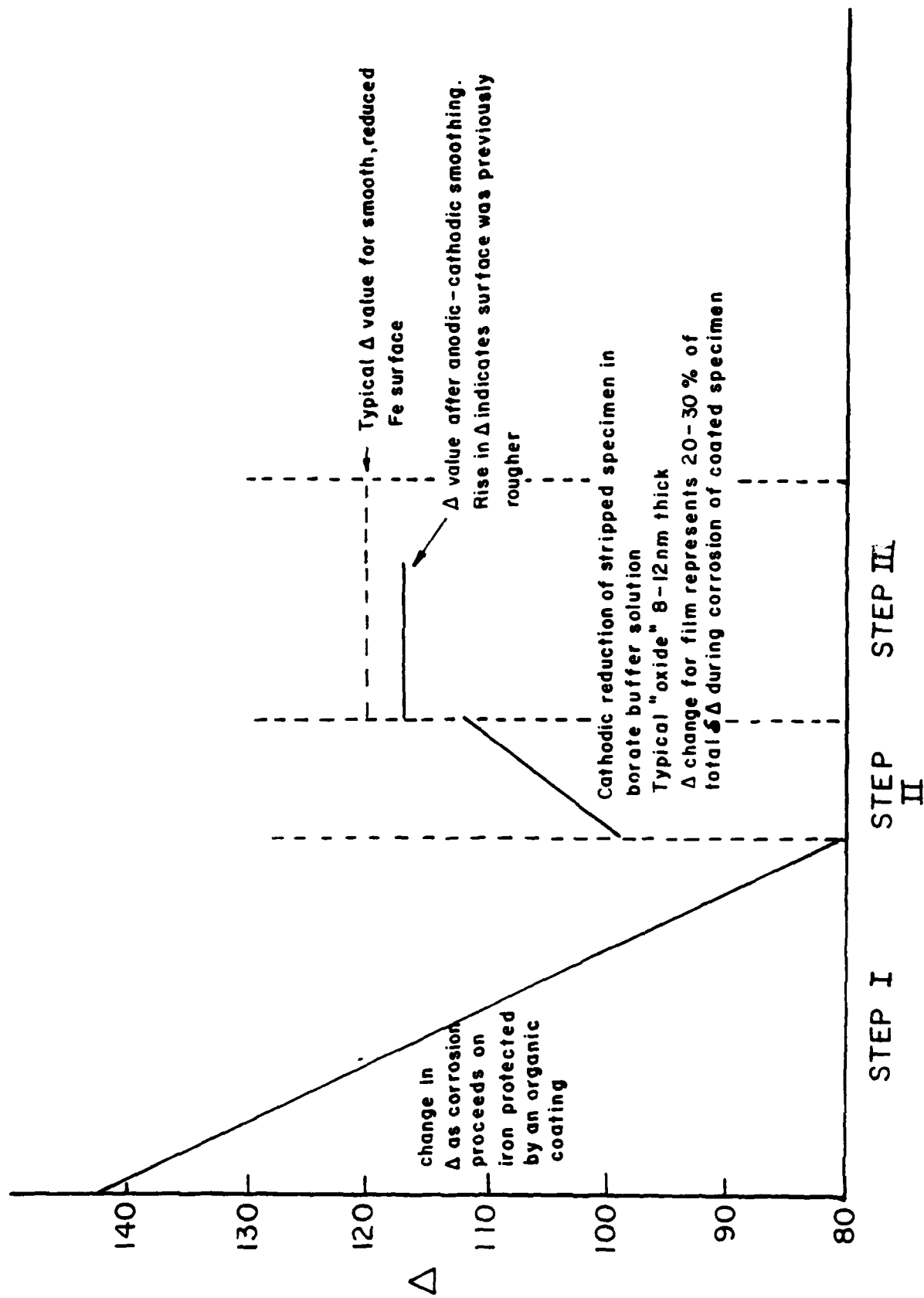


Figure 3

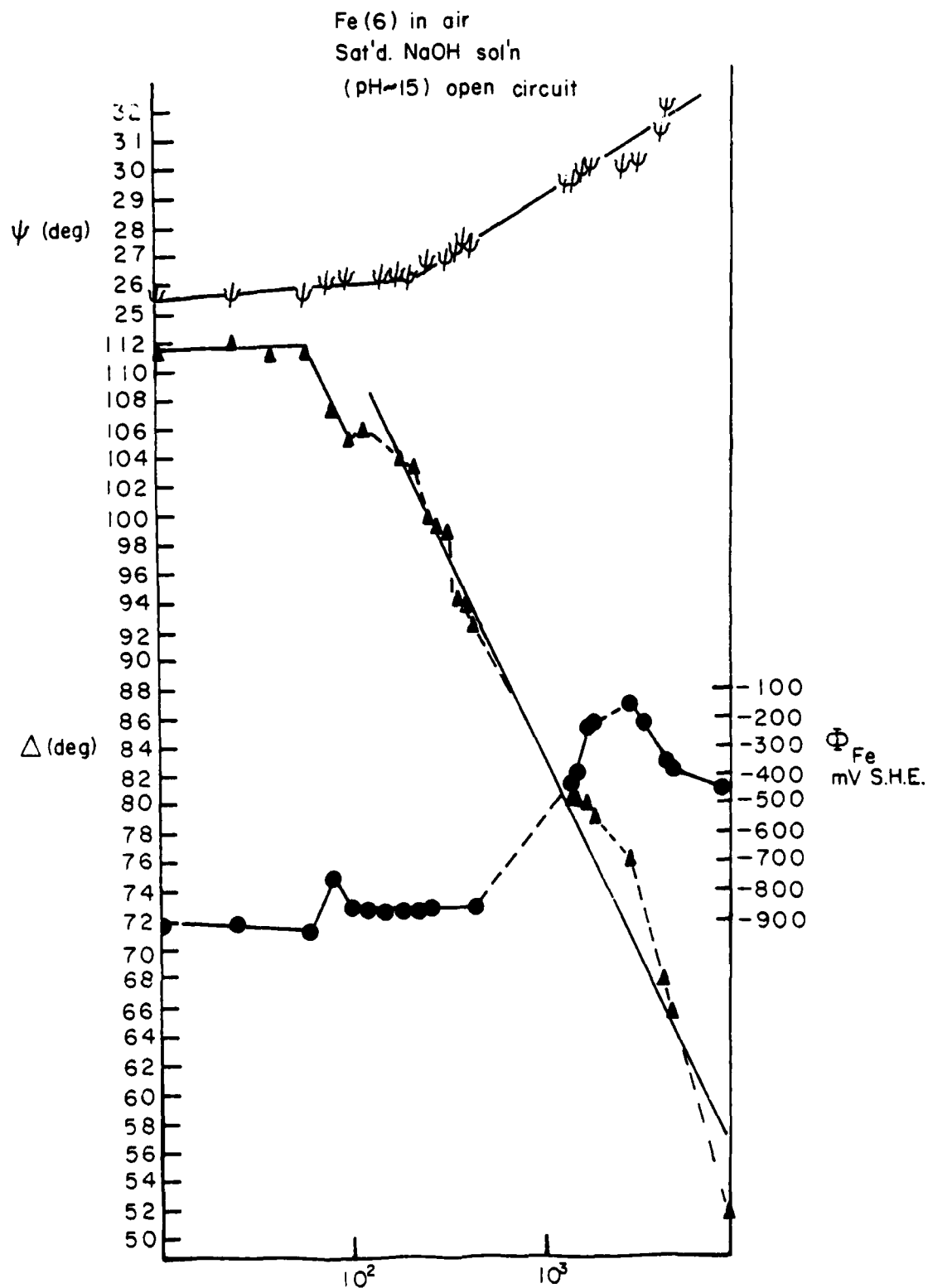
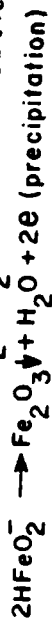
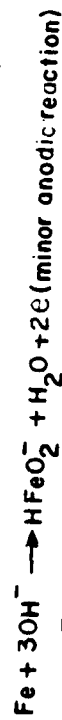
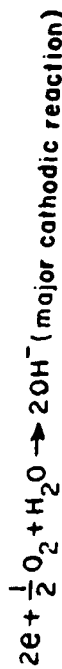


Figure 4



### CATHODIC REGION



### ANODIC REGION

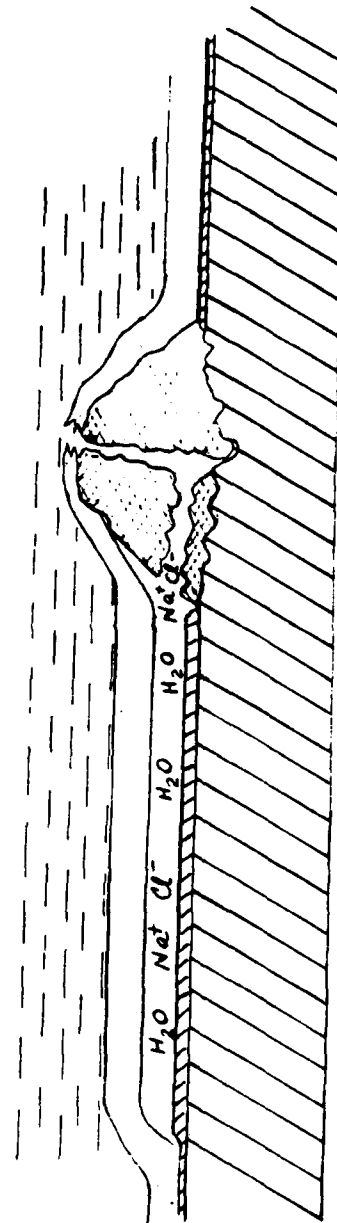
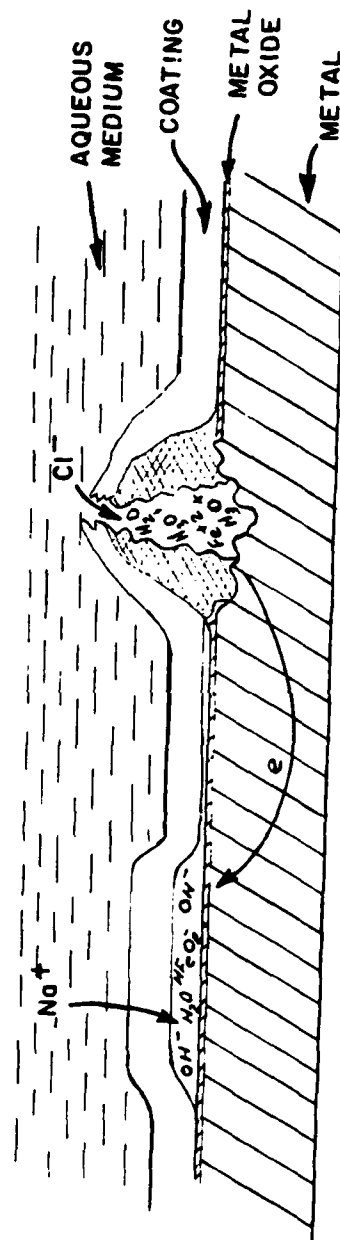
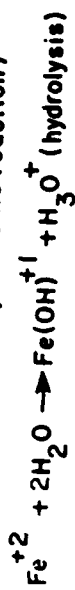


Figure 5

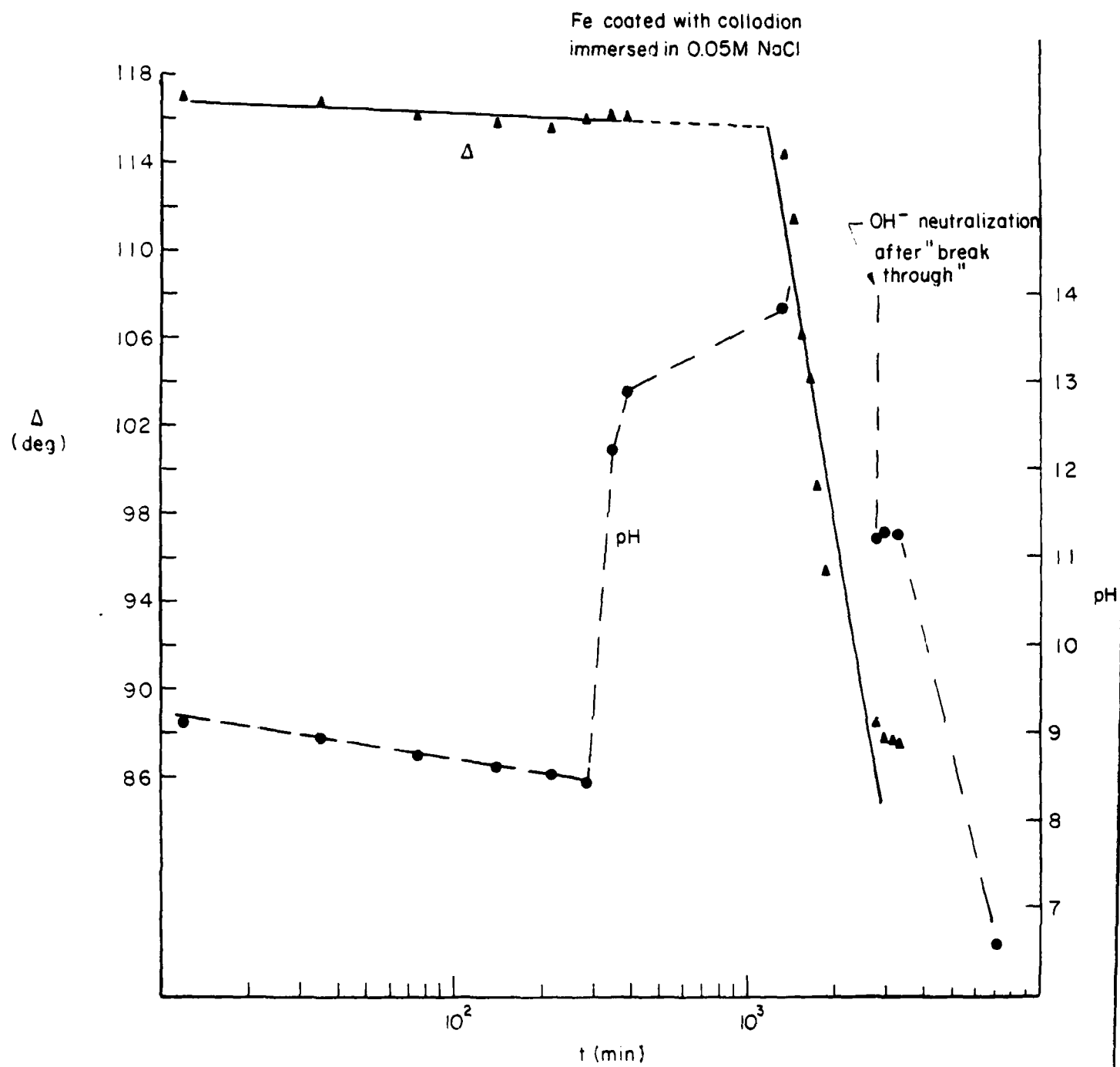


Figure 6

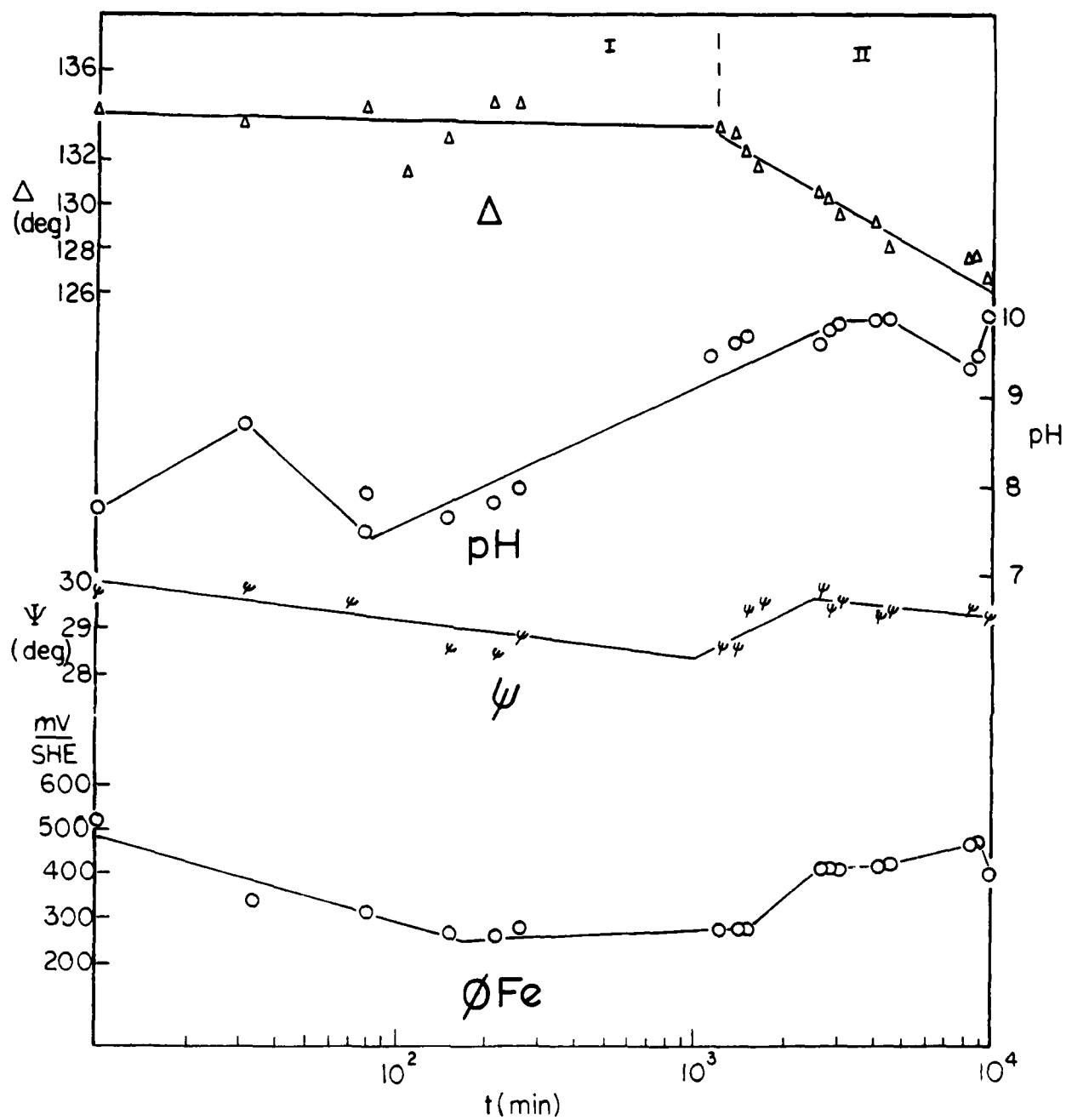


Figure 7

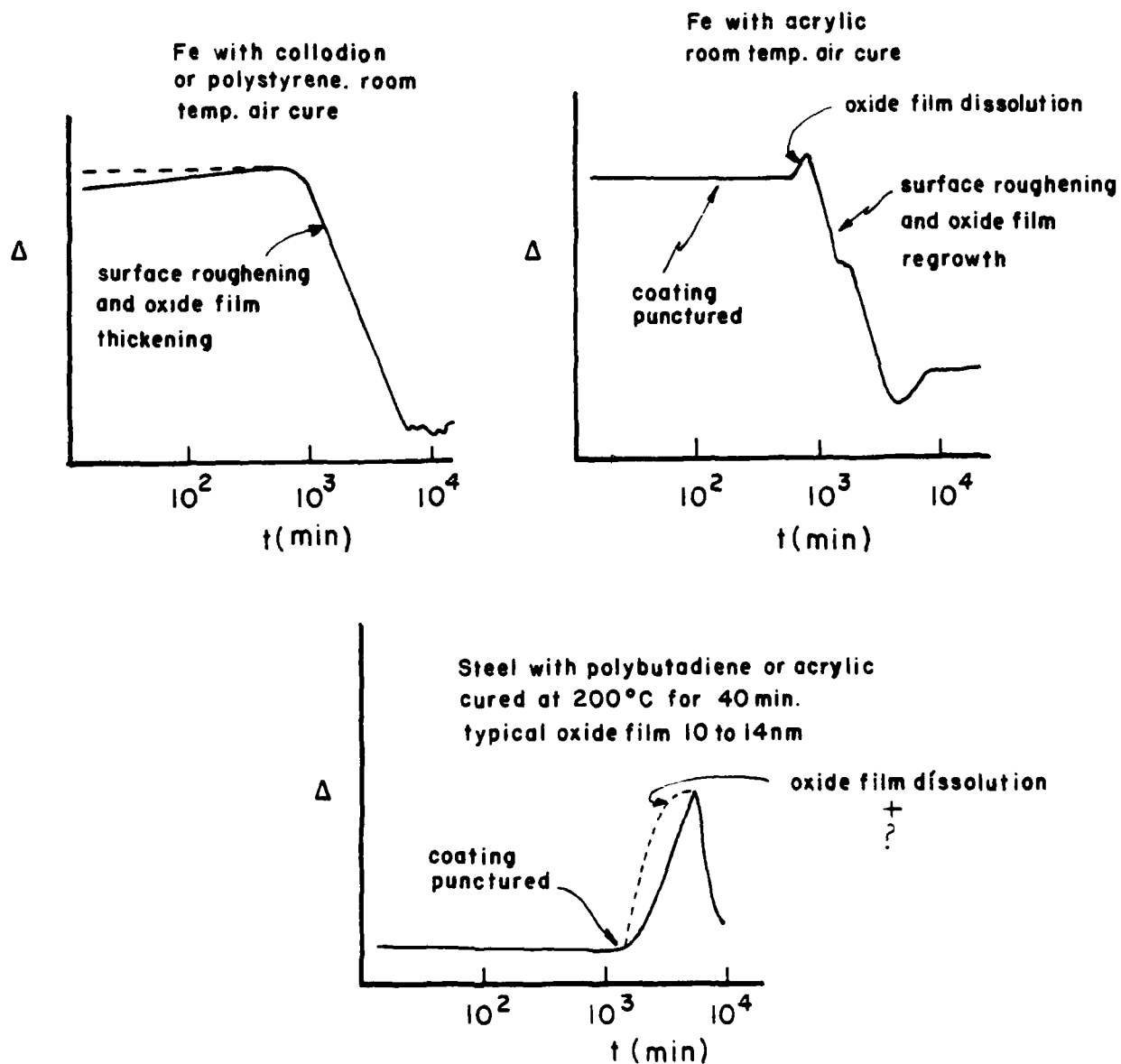


Figure 8

PART III. Accepted for publication as an accelerated brief communication by  
J. Electrochemical Society.

EXAFS Study of the Passive Film on Iron

Gabrielle G. Long, Jerome Kruger<sup>\*</sup>, David R. Black<sup>\*\*</sup>, and Masao Kuriyama

Center for Materials Science  
National Bureau of Standards  
Washington, D.C. 20234

<sup>\*</sup> Member of the Electrochemical Society

<sup>\*\*</sup> Also at the Department of Physics, Colorado State University, Fort Collins, Co.

Recent Mössbauer studies (1,2) of the passive film on iron have emphasized the important role of water in the structure of the in situ thin film. In these experiments, the "disorder" in the structure of the film was shown to be very similar to that of "amorphous" iron (III) oxide or hydroxide. Ex situ measurements using electron diffraction (3) have generally concluded that the main protective film on iron was crystalline  $\text{Fe}_3\text{O}_4$  at the metal-oxide interface and  $\gamma\text{Fe}_2\text{O}_3$  at the oxide-air interface. These results taken together can be understood if the vacuum environment of the ex situ experiments caused water to be removed from the films, causing their crystallization.

Laboratory-EXAFS (extended x-ray absorption fine structure) measurements (4) were undertaken in an attempt to determine the structure of the passive film using a direct method that avoids the need for a vacuum environment. (Background references on EXAFS are given in (4)). These exploratory measurements, while not in situ, did not require exposure of the films to a vacuum environment, and can be considered as intermediate, non-equilibrium results with respect to possible water in the film. These are the first results for the short range order parameters in the passive film, derived from measurements in a non-vacuum environment. Such information cannot be obtained directly from Mössbauer measurements.

The samples were 5 nm thick iron films vapor deposited on glass. They were passivated by immersing them in either a potassium chromate (0.005M) or a sodium nitrite (0.1M) passivating solution. Films formed this way have been shown (3,5) to have the structure, composition, and formation kinetics of the passive layers that form in  $\text{Fe}^{++}$ -free solutions by anodic oxidation.

The passive film experiment, which is a fluorescence-EXAFS measurement, utilizes a photocathode x-ray ionization chamber described earlier (6,7). The detector collects electrons emitted from the sample and amplifies them through field-intensified ionization in helium gas.

Transmission-EXAFS measurements were performed on (greater than 98% pure) finely powdered  $\text{Fe}_3\text{O}_4$ ,  $\gamma\text{Fe}_2\text{O}_3$ , and  $\gamma\text{FeO}(\text{OH})$ , and on (99.998% pure) bulk iron. These were then used as model compounds for the determination of phase shifts in the analysis of the thin films.

The iron-to-oxygen bond distances which were derived for the passive films are  $1.91 \pm 0.05$  and  $1.99 \pm 0.05$  Å for the nitrite-passivated and the chromate-passivated films respectively. These values are in the middle of the range of Fe-O and Fe-OH bond

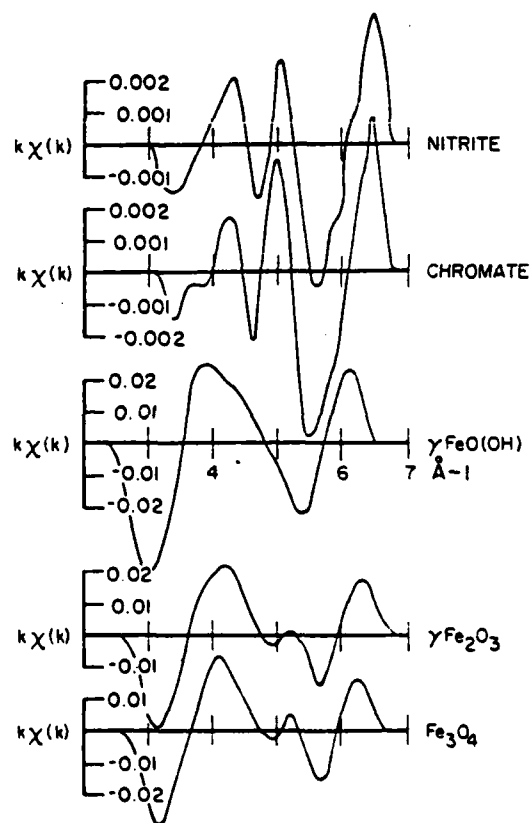


Figure 1. EXAFS signals ( $k\chi(k)$ ) for  $\gamma\text{Fe}_2\text{O}_3$ ,  $\text{Fe}_3\text{O}_4$ ,  $\gamma\text{FeO}(\text{OH})$  and the passive films. Note that only  $\gamma\text{FeO}(\text{OH})$  has two oscillations over this region in  $k$ -space.

lengths derived for the model compounds. The first iron-to-iron distances derived for the passivated films are shorter than those for  $\text{Fe}_3\text{O}_4$  and  $\gamma\text{Fe}_2\text{O}_3$ , and similar to that for  $\gamma\text{FeO(OH)}$ . It is useful to examine the EXAFS signal directly. Since  $\text{Fe}_3\text{O}_4$  and  $\gamma\text{Fe}_2\text{O}_3$  are both cubic spinels, where the latter is a defect version of the former, the EXAFS signals from these compounds should be quite similar. The  $\text{FeO(OH)}$  compounds are orthorhombic with a tetramolecular unit cell, and thus their EXAFS signals should be different from the spinel-like iron oxides. The EXAFS signal,  $k\chi(k)$ , over the range from  $k=3$  to  $k=7 \text{ \AA}^{-1}$  for the two sets of passive films are compared to those for the model compounds in Figure 1. The EXAFS signatures of the thin films are different from that of  $\gamma\text{FeO(OH)}$ , whereas they bear some resemblance to the signatures of the cubic spinels.

The magnitudes of the inverse Fourier transforms are shown for the crystalline iron oxides and iron hydroxide in Figure 2, and those for the passive films are shown in Figure 3. As indicated above, the positions of the first peaks (related to the Fe-O distance) in the passive films are very similar to positions for the crystalline compounds, whereas the positions of the second peaks (Fe-Fe distance) are different. Further, the amplitude ratios of the first to the second peak for the passive films are unlike

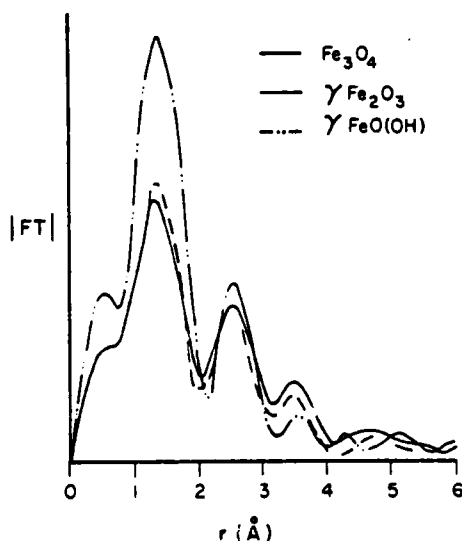


Figure 2. The magnitude of the inverse Fourier transform as a function of the radial distance,  $r$ , from the iron atom for the model crystalline compounds.

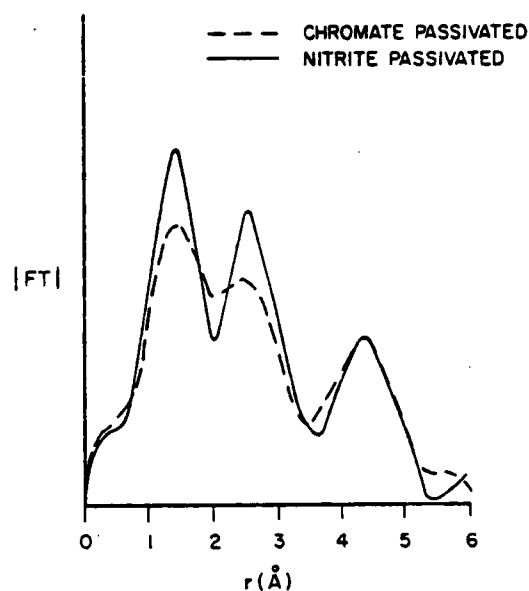


Figure 3. The magnitude of the inverse Fourier transform as a function of the radial distance,  $r$ , from the iron atom for the two passive films. The origin of the third peak is explained in Ref. 10.

those for the crystalline compounds. Since the data range in  $k$ -space used was as nearly identical as possible, this alteration in amplitude ratio may indicate a relative change in the number of nearest neighbors as well. This demonstrates that the passive film on iron is either different from these model compounds or a random mixture of many crystalline forms.

Although it has been shown that the structures of the nitrite-passivated and the chromate-passivated films are quite similar, the first two peaks in  $r$ -space are better resolved for the nitrite-formed film. This suggests that there may be a greater range of structures in the chromate-formed film, indicating greater disorder for this case. If the two films had the same structure in an aqueous environment, then the evident disorder in the chromate-passivated film could be the result of the improved stability of that film in the helium environment due to the inclusion of chromium (8). It was found, using a comparison of the fluorescence intensities at the chromium and the iron K-absorption edges, that more than 12% of

the cations in the film were chromium.

Furthermore, the absorption edge shift, as measured from the position of the K-edge of pure iron, was greatest for  $\gamma\text{Fe}_2\text{O}_3$ . If the passive films consist only of iron (III) compounds, the smaller edge shifts measured for the films would be evidence of a greater degree of covalency in the bonding (9). Another interpretation is that there may be both  $\text{Fe}^{++}$  and  $\text{Fe}^{+++}$  oxidation states present in the passive film, with the possibility of greater covalency as well. The smallest edge shift was found for the chromate-passivated film. This result taken together with the detection of Cr in this film suggests that it is the more vitreous of the two (8).

In conclusion, the EXAFS signatures of the passive films measured here resemble those of the cubic spinel ferric oxides. The sharpness of the peaks, however, is different, and at least the chromate-formed film may be more vitreous than the model crystalline compounds.

A complete account of the experiment and data analysis is to be published (10).

#### ACKNOWLEDGMENT

The contribution of J. Kruger was supported by the Office of Naval Research under contract NAOHR 18-69 NR036-082.

#### REFERENCES

1. W. E. O'Grady, *This Journal* **127**, 555 (1980).
2. J. Eldridge, M. E. Kordes and R. W. Hoffman, *J. Vac. Sci. Tech.* **20**, 934 (1982).
3. C. L. Foley, J. Kruger and C. J. Bechtoldt, *This Journal* **114**, 994 (1967).
4. G. G. Cohen, D. A. Fischer, J. Colbert and N. J. Shevchik, *Rev. Sci. Inst.* **51**, 273 (1980).
5. J. Kruger, *This Journal* **110**, 654 (1963).
6. N. J. Shevchik and D. A. Fischer, *Rev. Sci. Inst.* **50**, 577 (1979).
7. D. A. Fischer, G. G. Cohen and N. J. Shevchik, *J. Phys. F* **10**, L139 (1980).
8. A. G. Revesz and J. Kruger, *Passivity of Metals*, R. P. Frankenthal and J. Kruger, Eds., The Electrochemical Society, Princeton, NJ, 137 (1978).
9. I. A. Ovsyannikova, S. S. Batsanov, L. I. Nasanova, L. R. Batsanova, and E. A. Nekrasova, *Bull. Acad. Sci. USSR, Phys. Ser.* (English translation) **31**, 936 (1967).
10. Proceedings of the "International Conference on the Electronic and Molecular Structure Of the Electrode-Electrolyte Interface, held in Logan, Utah, July 25-30, 1982. To be published in *J. Electroanal. Chem.*



Structure of Passive Films on Iron Using a New Surface-EXAFS Technique

by

G.G. Long, J. Kruger, D.R. Black\* and M. Kuriyama

Metallurgy Division  
Center for Materials Science  
National Bureau of Standards  
Washington, DC 20234

ABSTRACT

There exists considerable controversy about the structure, the bonding, and the composition of the passive films that form on iron surfaces in aqueous electrolytes. A major problem is that most of the surface analytical techniques used to characterize the passive film require exposure to vacua, which can alter the structure of the passive film. This study seeks to overcome this problem through the application of a new surface-EXAFS (extended x-ray absorption fine structure) technique that is both extremely sensitive to structural and bonding changes in the 2 to 3 nm passive film and does not require the use of a vacuum environment.

Near edge and extended x-ray absorption fine structure spectra from passive films on iron were measured and compared with those from pure iron and a polycrystalline iron oxide of known structure. The EXAFS data provide a measure of the relative disorder in the passive films, and they were used to derive bond lengths for the iron-to-oxygen and the iron-to-iron coordination shells. It was found that there was greater disorder in a chromate formed film than in a nitrite formed film. The iron-to-oxygen bond lengths were within the usual range for the crystalline iron oxides but the iron-to-iron distances corresponded to none of the known structures. The near-edge data reveal differences in the electronic configurations of passive film samples formed in different aqueous electrolytes.

\*Also at the Department of Physics, Colorado State University,  
Fort Collins, Colorado

## INTRODUCTION

Passivity is a crucial factor in determining the capability of a metal to resist environmental attack. (See [1] for a comprehensive review.) The nature and structure of the passive film that is responsible for this phenomenon has been a key focus of efforts aimed at developing an understanding of passivity. There have been a number of attempts to determine the nature and structure of the passive film, especially on iron [1]. For example, electron diffraction experiments [2] found that the passive film on iron was crystalline  $\gamma\text{-Fe}_2\text{O}_3$ . Other surface analytical approaches have also been used, such as Auger electron spectroscopy [3] and photoelectron spectroscopy [4]. It is often concluded that the main protective film on iron is cubic  $\text{Fe}_3\text{O}_4$  at the metal-to-oxide interface, and  $\gamma\text{-Fe}_2\text{O}_3$  and hydrated oxides at the film-to-air interface.

These conclusions have been criticized by O'Grady [5], who suggested that previous attempts used techniques that required ex situ examination of the passive film on iron in a vacuum, which could remove the water or hydrogen-containing species from the films and cause their crystallization. O'Grady, using in situ Mossbauer spectroscopy, found that the passive layers on iron were iron (III) oxides arranged in polymeric chains. When these films were dried by exposure to a vacuum, they appeared to be composed of polycrystalline  $\gamma\text{-Fe}_2\text{O}_3$ .

The work described here attempts to exploit, for the first time, the opportunities provided by a new surface-EXAFS (extended x-ray absorption fine structure) technique [6,7] to extract information about the passive film on iron in a non-vacuum environment. The technique is capable of supplementing O'Grady's findings by providing parameters on the specific structure and composition of the film.

The bonding flexibility, which arises from the type of bonding in the film, is another important factor in the quality of passivation. The role of partially ionic and partially covalent bonds in the formation of stable glassy structures has been discussed by Myuller [8]. In this work, the degree of covalency of the iron to oxygen bonds in the passive film is investigated through a study of the K-absorption edge threshold and the effective "coordination charge" of the thin films.

### EXPERIMENT AND DISCUSSION

The samples were 5 nm thick iron films vapor-deposited on glass. They were passivated by immersing them in either a chromate (0.005 M) or a nitrite (0.1 M) passivating solution. Near edge and extended x-ray absorption fine structure spectra were measured on these films, as well as on foils of pure iron and on purified  $\text{Fe}_3\text{O}_4$  powder.

The K-absorption spectrum for pure iron shows a rounded absorption edge, as is usual for a transition metal, and that for  $\text{Fe}_3\text{O}_4$  is sharply peaked. These two spectra, shown in Figure 1, were measured in the transmission EXAFS geometry, using a tunable laboratory EXAFS system described elsewhere [9]. The positions of the K-edges were determined from the known dispersion of the monochromator and from Fe  $K\beta_{1,3}$  and Ni  $K\alpha$ ,  $K\alpha_2$  lines which were present due to impurities in the rotating anode x-ray target. The latter pair of lines effectively ended our EXAFS data set about 360 eV above the Fe edge.

Transmission geometry EXAFS is not generally sufficiently sensitive to the surface layers to be useful for a surface-EXAFS measurement. A fluorescence-EXAFS technique is required. It is desirable to collect only those photons or electrons that originate in the surface region. The passive film experiment makes use of a photocathode x-ray ionization

chamber. This detector was especially developed for surface-EXAFS [6], and was demonstrated to be sensitive to the oxidation processes in metallic copper [7]. The detector collects electrons emitted from the sample (which serves as the cathode plate) and amplifies them through field intensified ionization in helium gas. Since the electrons emerging from the sample must create electron-ion pairs in the gas, and the ionization potential of helium is  $\sim 30$  eV, the detector weights the higher energy electrons more strongly than the lower energy ones. Near the absorption threshold, the photoelectron energy is low and not able to yield much detector current. The Auger electron, created by the decay of the core hole, is substantially more energetic and able to produce a much larger signal. The glass substrate absorbs x-rays passing into it far from the photocathode overlayer, and so contributes little to the current.

The absorption spectra for the chromate- and the nitrite-passivated films are shown in Figure 2. The raw data for the two sets of films are quite similar with the important exceptions of the positions of the absorption threshold and the near-edge fine structures. The nitrite formed film shows evidence of an enhancement in the near-edge absorption coefficient that is suppressed in the chromate-formed film. This is evidence of a difference in the density distribution of empty or partially-empty molecular orbitals in the two films. This near-edge enhancement [10] in the K-absorption spectrum of the nitrite-formed film indicates that it has an increased density of available final states of p-character.

Further evidence of differences in the electronic structure of the two films comes from the measured positions of the inflection points of their iron K-edges. The positions and energy shifts measured in this work for pure Fe,  $\text{Fe}_3\text{O}_4$ , and the two passivated films are given in Table 1, along

with energy shifts for FeO and Fe<sub>2</sub>O<sub>3</sub> measured by Chen [11]. The observed energy shifts reflect changes in the charge distribution of the valence band, the degree of ionicity, and the coordination number. This effect can be described by the effective "coordination charge," which is given by

$$n = m - \sum_K n_K C_K$$

where  $m$  is the oxidation plate,  $C_K$  is the degree of covalence of a bond ( $C_K = 1 - i_K$  where  $i_K$  is the ionicity), and  $n_K$  is the number of such bonds. There is a nearly linear relationship between  $\Delta E$  ( $= E_{\text{compound}} - E_{\text{metal}}$ ), the energy shift, and the coordination charge of the compound [13,14].

The effective coordination charge for Fe<sub>3</sub>O<sub>4</sub> was calculated using the ionicities for FeO and Fe<sub>2</sub>O<sub>3</sub> derived from Levine [14] and the structure as determined by Shull et al. [15] using neutron diffraction. (One third of the iron cations are trivalent and tetrahedrally coordinated, one third are divalent and octahedrally coordinated, and the remainder are trivalent and octahedrally coordinated.) Our result for Fe<sub>3</sub>O<sub>4</sub>, and Chen's [11] for FeO and Fe<sub>2</sub>O<sub>3</sub>, are shown in Table 1. Assuming a linear relationship between  $\Delta E$  and  $n$ , the effective coordination charges for the passive films can be derived. There is a significantly lower coordination charge for the chromate-passivated film, indicating greater covalency in the bonding around the Fe in this film. This lends support to the idea that the chromate-passivating solution, which should introduce chromium into the passive film, can thereby, according to Revesz and Kruger [16], promote the formation of non-crystalline (glassy) passive films. A comparison of the edge step at the chromium and the iron edges for this film indicated that at least 12% of the cations in the film were chromium.

Up to this point, we have been considering the region in the absorption

spectrum from 0 to 30 eV above the edge. In this portion of the spectrum, the features are due to many body interactions and band effects. Recently, this region has been interpreted [17] also by a multiple scattering approach, which should be sensitive to bond angles, and as should prove to be important in the study of covalently bonded systems (e.g. glasses). Further work will attempt to exploit this new, still developing technique.

We next look at the EXAFS region, which in this work commences at ~35 eV and continues to ~360 eV above threshold. The oscillatory structure in this portion of the spectrum can be interpreted using the assumption that single scattering contributions dominate. This leads, in a straight forward way, to the determination of structural parameters [18]. The EXAFS data can be analyzed by taking a Fourier transform of the spectrum, properly weighted to allow for the backscattering amplitude and phase variations. Since we are interested in obtaining the Fe-O and the Fe-Fe bond lengths, this procedure would require taking two transforms, where the one would display peaks at the bond lengths  $r_j$  for Fe-O and the other would be used to find the  $r_j$  for Fe-Fe. Each would also show additional peaks, at incorrect positions, for the other type of bond. It was decided instead to calculate the Fourier transforms of the pure Fe and the Fe<sub>3</sub>O<sub>4</sub> data, and use their known structures to determine empirically the required phase factors. Since iron and oxygen are far apart in the periodic table, the backscattering amplitudes attributed to them are very different. These are shown in Figure 3, calculated from Teo and Lee [19]. It is evident that oxygen backscattering dominates at low energy ( $k$ ) and iron at high energy. The Fourier transforms of both sets of passive film data were dominated by the pure iron substrate when the transform was taken over a high  $k$  bandwidth. a low  $k$  bandwidth, however, yielded information dominated by the oxide film, with only the fourth shell Fe-Fe visible. Fourier frequencies

due to the lower shells in bulk Fe are not seen since the high k region, where they dominate, was omitted from the low k bandwidth.

The results for the magnitudes of the Fourier transforms for the passive film data are shown in Figure 4, and the Fe-O and Fe-Fe distances, corrected for phase shift, are given in Table 2. Uncertainties in these results are estimated to be  $\pm 0.05$  Å. As could be expected from the raw data, the geometric arrangement of the two films is quite similar. It is noteworthy, however, that using nearly identical Fourier resolution (i.e. the same range in k space, and the same sampling rate) for the two data sets, the first two peaks in r space are well resolved for the nitrite-passivated film and much less well-resolved for the chromate-passivated film. This suggests that, although the coordination for the two films is similar, there is a greater range of structural parameters (greater disorder) in the chromate-formed film, indicating greater disorder in this film. This result supports the suggestions of Revesz and Kruger [16] that the introduction of chromium, a glass former, into the passive film results in a more non-crystalline structure with bonds having a higher percent of covalency than films containing only iron, oxygen and hydrogen. The Fe-O distances for the thin films are in the range of the usual Fe-O and Fe-OH distances found in the iron oxides. The Fe-Fe distances determined here are significantly smaller than those found in  $\text{Fe}_3\text{O}_4$  or  $\gamma\text{-Fe}_2\text{O}_3$ , and they are larger than those of  $\alpha\text{-}$  and  $\gamma\text{-FeOOH}$ . Thus, the structure of the passive film does not really resemble these categories of crystalline oxides. This is supportive of the conclusions of O'Grady [5] that the structure of the passive film on iron resembles a polymeric film of hydrated iron oxide. But these results go one step further in that they add numerical parameters and place structural limitations on the suggested model.

### CONCLUSIONS

The usefulness of a new surface-EXAFS technique to examine 2-3 nm passive films on iron for composition, structure, and bonding characteristics has been demonstrated. Passive films formed on iron in nitrite and in chromate solutions show Fe-Fe distances different from those observed for the known iron oxides and oxy-hydroxides. The passive film formed on iron in a chromate solution shows bonding of a higher percentage of covalency than that formed by a nitrite solution. Furthermore, the chromate-formed film shows evidence of being more non-crystalline than the nitrite-formed film, and it was found that more than 12% of the cations in the chromate-formed film were chromium.

### ACKNOWLEDGEMENTS

We are very grateful to Drs. E. N. Farabaugh and D. M. Sanders for providing us with the thin film iron specimens. We also thank the Office of Naval Research for partial support under contract NAONR 18-69NR036-082.



## REFERENCES

1. R.P. Frankenthal and J. Kruger, Editors, Passivity of Metals, The Electrochemical Society, Princeton, 1978.
2. C.L. Foley, J. Kruger, and C.J. Bechtoldt, J. Electrochem. Soc., 114 (1967) 994.
3. M. Seo, J.B. Lumsden, and R.W. Staehle, Surf. Sci., 50 (1975) 541.
4. G. Okamoto, Corros. Sci., 13 (1973) 471.
5. W.F. O'Grady, J. Electrochem. Soc., 127 (1980) 555.
6. N.J. Shevchik and D.A. Fischer, Rev. Sci. Instrum. 50 (1979) 577.
7. D.A. Fischer, G.G. Cohen, and N.J. Shevchik, J. Phys. F, 10 (1980) L139.
8. R.L. Myuller, Solid State Chemistry, O.U. Borisova, Editor, (translated from Russian), Consultants Bureau, New York, 1966, p. 1.
9. G.G. Cohen, D.A. Fischer, J. Colbert and N.J. Shevchik, Rev. Sci. Instrum., 51 (1980) 273.
10. M. Brown, R.E. Peieris, and E.A. Stern, Phys. Rev. B 15 (1977) 738.
11. H. Chen, J. Phys. Chem. Solids, 41 (1980) 641.
12. I.A. Ovsyannikova, S.S. Batsanov, L.I. Nasonova, L.R. Batsanova, and E.A. Nekrasova, Bull. Acad. Sci., USSR Phys. Ser. (English translation) 31 (1967) 936.
13. S.P. Cramer, T.K. Eccles, F. Kutzler, K.O. Hodgson, and L.E. Mortenson, J. Am. Chem. Soc. 98 (1976) 1285.
14. B.F. Levine, J. Chem. Phys. 59 (1973) 1463.
15. C.G. Shull, E.O. Wollan and W.C. Koehler, Phys. Rev. 84 (1951) 912.
16. A.G. Revesz and J. Kruger, Passivity of Metals, R.P. Frankenthal and J. Kruger, Editors, The Electrochem. Soc., Princeton, 1978, p. 137.
17. P.J. Durham, J.B. Pendry and C.H. Hodges, Sol. St. Commun., 38 (1981) 159.

18. E.A. Stern, Phys. Rev. B, 10 (1974) 3027 F.W. Lytle, D.E. Sayers,  
and E.A. Stern, Phys. Rev. B 11 (1975) 4825.
19. B.K. Teo and P.A. Lee, J. Am. Chem. Soc., 101 (1979) 2815.

TABLE I

Positions of the Fe K-edges and the calculated effective coordination charges

Sample	K-edge (eV)	$\Delta E$ (eV)	n
pure Fe	7112	0	
Fe <sub>0.905</sub> O <sup>a</sup>		5 <sup>a</sup>	1.238 <sup>a</sup>
Fe <sub>3</sub> O <sub>4</sub>	7121	9	1.920
$\gamma$ -Fe <sub>2</sub> O <sub>3</sub>		11	2.0031
nitrite passivated film	7120	8	1.670
chromate passivated film	7117	5	1.238

<sup>a</sup>From reference [11].

Table 2  
Bond type versus bond distance in Ångstroms

Bond type	Fe <sub>3</sub> O <sub>4</sub> <sup>a</sup>	αFeOOH <sup>b</sup>	nitrite	chromate
Fe - O	1.82 2.10	1.94 2.13	2.02	2.09
Fe - OH		2.05		
Fe - Fe	2.97 3.46 3.63	2.88	3.27	3.18

<sup>a</sup>Calculated using the space group  $O_h^7$  (Fd3m) with  $u = 0.379$  and  $a = 8.396 \text{ Å}$ .  
R. W. G. Wyckoff, Crystal Structures, 2<sup>nd</sup> Edition, Vol. 3, J. Wiley,  
New York, 1965.

<sup>b</sup>R. W. G. Wyckoff, Crystal Structures, 2<sup>nd</sup> Edition, Vol. 1, J. Wiley,  
New York, 1963.

#### FIGURE CAPTIONS

- Figure 1. X-ray absorption spectra for iron and  $\text{Fe}_3\text{O}_4$ .
- Figure 2. X-ray absorption spectra for the thin films, showing an edge enhancement in the nitrite-formed film.
- Figure 3. Backscattering amplitudes for iron and oxygen, as a function of  $k$ .
- Figure 4. The magnitude of the Fourier transform versus  $q$  for the nitrite- and chromate-passivated films. Both were calculated from the low  $k$  region of the data.

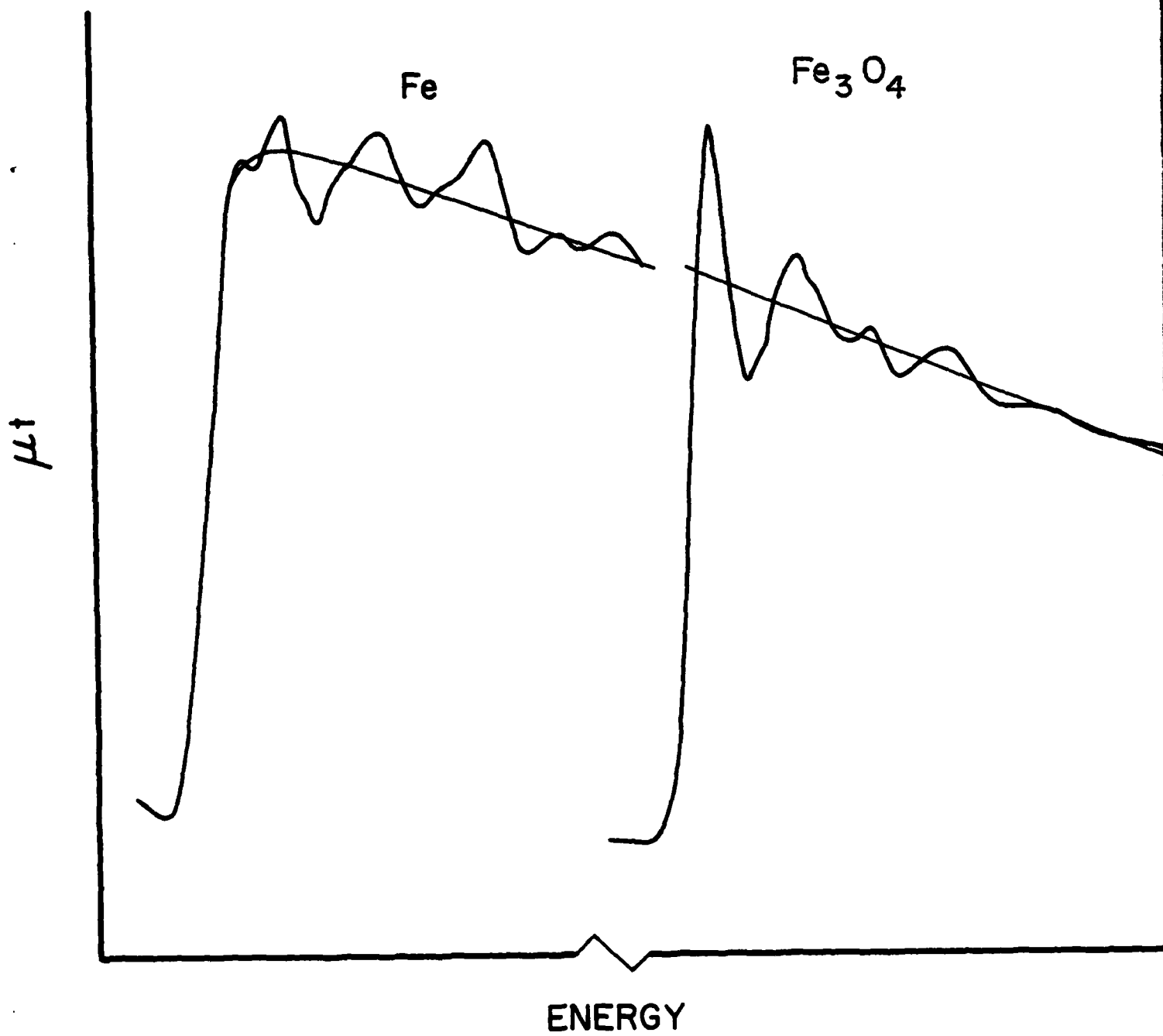


FIG 1

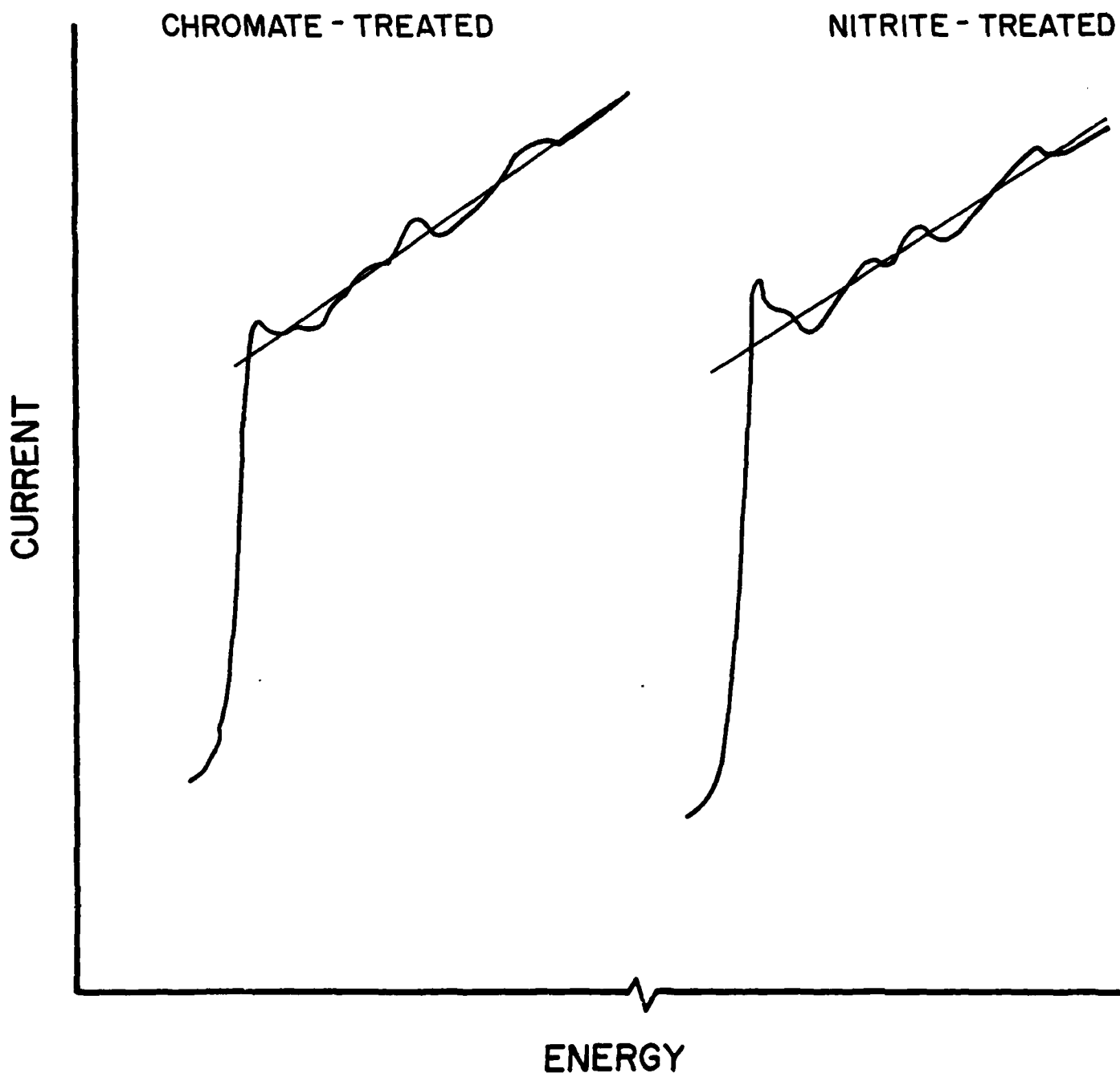


FIG 2

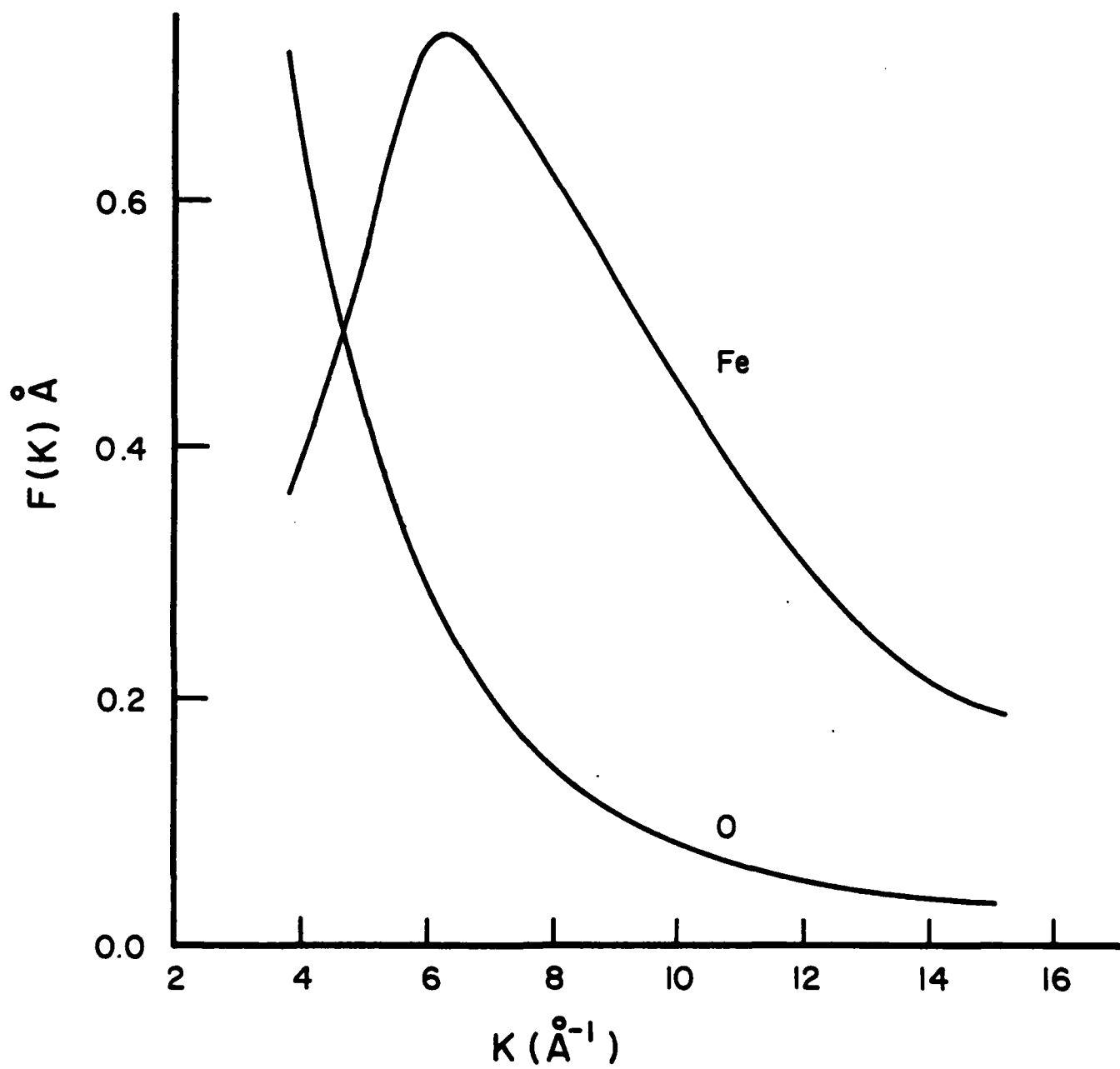


FIG 3



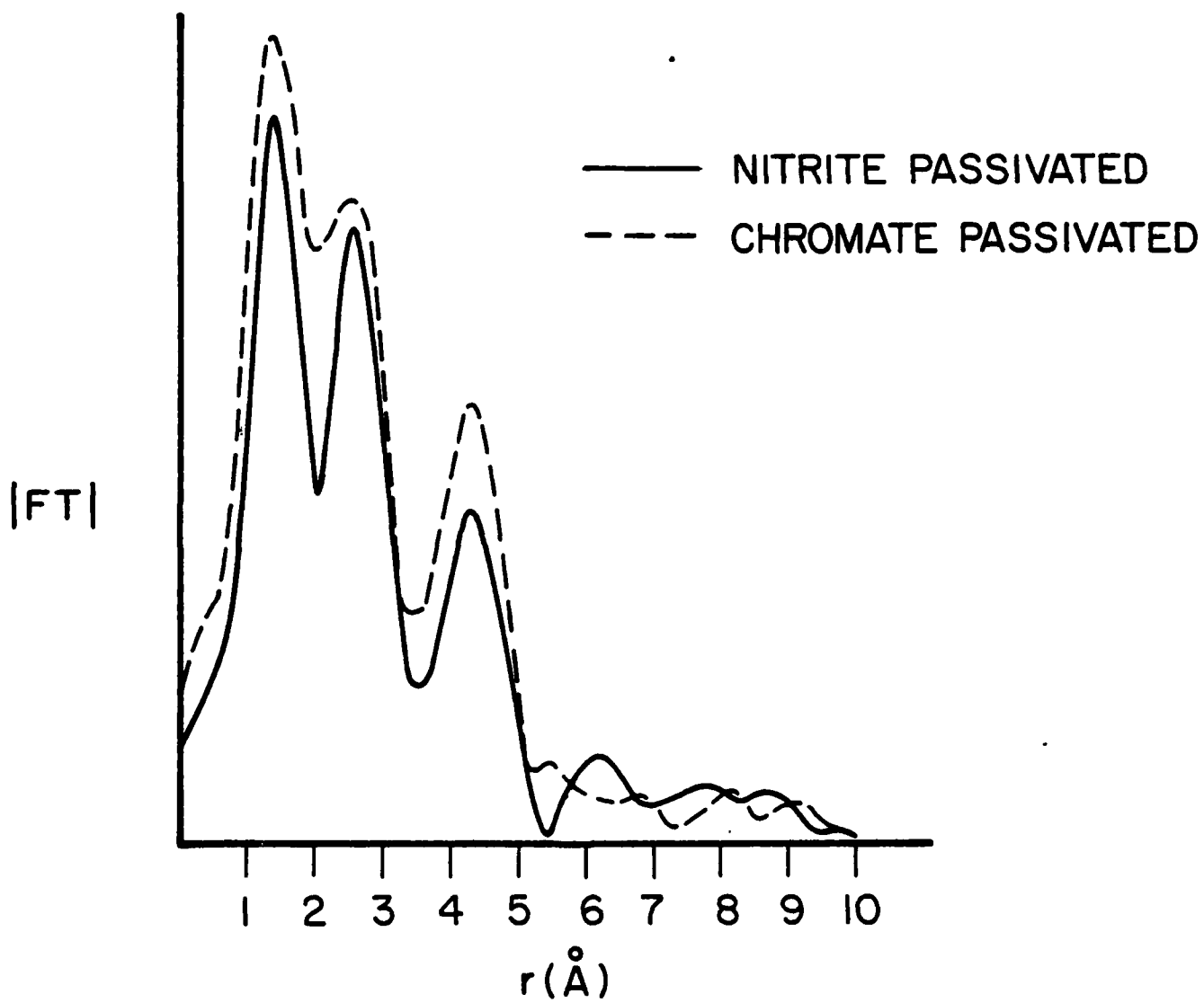
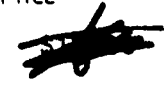


FIG 4

U.S. DEPT. OF COMM. <b>BIBLIOGRAPHIC DATA SHEET</b> (See instructions)	1. PUBLICATION OR REPORT NO. NBSIR-83-2551 <sup>1</sup>	2. Performing Organ. Report No. AD-A124879	3. Publication Date February 1983
4. TITLE AND SUBTITLE <p style="text-align: center;">PASSIVE FILMS, SURFACE STRUCTURE, AND STRESS CORROSION AND CREVICE CORROSION SUSCEPTIBILITY</p>			
5. AUTHOR(S) <p style="text-align: center;">J. Kruger, J. J. Ritter, and G. G. Long</p>			
6. PERFORMING ORGANIZATION (If joint or other than NBS, see instructions) NATIONAL BUREAU OF STANDARDS DEPARTMENT OF COMMERCE WASHINGTON, D.C. 20234			7. Contract/Grant No. NAONR-18-69 NRO 36-082 8. Type of Report & Period Covered
9. SPONSORING ORGANIZATION NAME AND COMPLETE ADDRESS (Street, City, State, ZIP) Office of Naval Research Arlington, Virginia 22217			
10. SUPPLEMENTARY NOTES  <input type="checkbox"/> Document describes a computer program; SF-185, FIPS Software Summary, is attached.			
11. ABSTRACT (A 200-word or less factual summary of most significant information. If document includes a significant bibliography or literature survey, mention it here) <p>Parts I and II: Transparent organic coatings on iron and steel are used to simulate painted metal surfaces for simultaneous ellipsometric and electrochemical measurements. The studies have revealed that significant changes in the interfacial oxide layer occur as corrosion proceeds. These changes have been, in part, attributed to a dissolution of the interfacial oxide and this phenomenon is identified as one mechanism of cathodic coating delamination. Additional phenomena such as surface roughening, oxide film regrowth, and spatial development of cathodes are discussed. The effects of coating cure and the presence of inhibitors are also presented.</p> <p>Parts III and IV: The bonding, structure, and composition of passive films are still controversial subjects. A new surface EXAFS technique, capable of probing a passive film on iron in its native aqueous environment has been applied to this problem. The studies show that Fe-Fe distances for passive films formed in nitrite and chromate solutions are different from those of known iron oxides and oxyhydroxides. Moreover, differences in the degree of covalency of iron and in the crystallinity of these films have also been detected.</p>			
12. KEY WORDS (Six to twelve entries; alphabetical order; capitalize only proper names; and separate key words by semicolons) Chromates; corrosion; electrochemistry; ellipsometry; EXAFS, Fe-Fe bond lengths; iron; nitrites; organic coatings; oxide films; passivation			
13. AVAILABILITY <input checked="" type="checkbox"/> Unlimited <input type="checkbox"/> For Official Distribution, Do Not Release to NTIS <input type="checkbox"/> Order From Superintendent of Documents, U.S. Government Printing Office, Washington, D.C. 20402. <input checked="" type="checkbox"/> Order From National Technical Information Service (NTIS), Springfield, VA. 22161			14. NO. OF PRINTED PAGES 70 15. Price 

END